Title

A multiscale computational modelling approach predicts mechanisms of female sex risk in the setting of arousal-induced arrhythmias

Permalink

https://escholarship.org/uc/item/9v21b3h1

Journal

The Journal of Physiology, 595(14)

ISSN

0022-3751

Authors

Yang, Pei-Chi
Perissinotti, Laura L
López-Redondo, Fernando
et al.

Publication Date

2017-07-15

DOI

10.1113/jp273142

Peer reviewed

A multiscale computational modelling approach predicts mechanisms of female sex risk in the setting of arousal-induced arrhythmias

Pei-Chi Yang[1], Laura L. Perissinotti[2], Fernando López-Redondo[3], Yibo Wang[2], Kevin R. DeMarco[1], Mao-Tsuen Jeng[1], Igor Vorobyov[1], Robert D. Harvey[4], Junko Kurokawa[3,5], Sergei Y. Noskov[2] and Colleen E. Clancy[1] (ID)

[1] *Department of Pharmacology, School of Medicine, University of California, Davis, CA, USA*
[2] *Centre for Molecular Simulation, Department of Biological Sciences, University of Calgary, Alberta, Canada*
[3] *Department of Bio-informational Pharmacology, Medical Research Institute, Tokyo Medical and Dental University*
[4] *Department of Pharmacology, University of Nevada, Reno, NV, USA*
[5] *Department of Bio-informational Pharmacology, School of Pharmaceutical Sciences, University of Shizuoka, Shizuoka, Japan*

The Journal of Physiology

Key points

- This study represents a first step toward predicting mechanisms of sex-based arrhythmias that may lead to important developments in risk stratification and may inform future drug design and screening.
- We undertook simulations to reveal the conditions (i.e. pacing, drugs, sympathetic stimulation) required for triggering and sustaining reentrant arrhythmias.
- Using the recently solved cryo-EM structure for the Eag-family channel as a template, we revealed potential interactions of oestrogen with the pore loop hERG mutation (G604S).
- Molecular models suggest that oestrogen and dofetilide blockade can concur simultaneously in the hERG channel pore.

Abstract Female sex is a risk factor for inherited and acquired long-QT associated torsade de pointes (TdP) arrhythmias, and sympathetic discharge is a major factor in triggering TdP in female long-QT syndrome patients. We used a combined experimental and computational approach to predict 'the perfect storm' of hormone concentration, I_{Kr} block and sympathetic stimulation that induces arrhythmia in females with inherited and acquired long-QT. More specifically, we developed mathematical models of acquired and inherited long-QT syndrome in male and female ventricular human myocytes by combining effects of a hormone and a hERG blocker, dofetilide, or hERG mutations. These 'male' and 'female' model myocytes and tissues then were used to predict how various sex-based differences underlie arrhythmia risk in the setting of acute sympathetic nervous system discharge. The model predicted increased risk for arrhythmia in females when acute sympathetic nervous system discharge was applied in the settings of both inherited and acquired long-QT syndrome. Females were predicted to have protection from arrhythmia induction when progesterone is high. Males were protected by the presence of testosterone. Structural modelling points towards two plausible and distinct mechanisms of oestrogen action enhancing torsadogenic effects: oestradiol interaction with hERG mutations in the pore loop containing G604 or with common TdP-related blockers in the intra-cavity binding site. Our study presents findings that constitute the first evidence linking structure to function mechanisms underlying female dominance of arousal-induced arrhythmias.

Abbreviations   APD, action potential duration; BCL, basic cycle length; DHT, dihydrotestosterone; E2, oestradiol; EAD, early afterdepolarization; hERG, human *ether-à-go-go*-related gene; I_{Ks}, slow delayed rectifier K$^+$ current; I_{Ca-L}, inward Ca^{2+} current,; ISO, isoproterenol; MD, molecular dynamics; OA, okadaic acid; Pg, progesterone; PKA, protein kinase A; QTc, corrected QT; SNS, sympathetic nervous system; TdP, torsade de pointes.

Introduction

Cardiac arrhythmia is a primary cause of mortality in both males and females, but the risk factors associated with some types of arrhythmias differ between the sexes. Female sex is the dominant risk factor for acquired long-QT-dependent arrhythmias after puberty, with at least 70% incidence in females (Makkar *et al.* 1993). Despite recognition of this fact, the specific mechanisms underlying sex-based differences in humans are notably understudied and have not been comprehensively revealed (Tadros *et al.* 2014; Salama & Bett, 2014). Clinical and experimental data uniformly agree that women have longer QT intervals than men and are more likely to develop long-QT-dependent arrhythmias such as torsade de pointes (TdP) (Lehmann *et al.* 1996; Pham *et al.* 2001; Rodriguez *et al.* 2001; Pham *et al.* 2002; Salama & Bett, 2014) that can degenerate into sudden cardiac death. Women are also susceptible to *acquired* long-QT syndrome, resulting from block of the cardiac repolarizing rapidly activating delayed rectifier K$^+$ current (I_{Kr}), through the human *ether-à-go-go*-related gene (hERG) channel arising from the *KCNH2* gene.

The longer QT interval observed in women is attributed to a reduced repolarization reserve (James *et al.* 2007). Recent clinical and experimental studies suggest that this is due to the non-genomic effects that sex steroid hormones have on the electrical properties of the heart (Burke *et al.* 1997; Rodriguez *et al.* 2001; Bai *et al.* 2005; Liu *et al.* 2005; Nakagawa *et al.* 2006; Nakamura *et al.* 2007; Kurokawa *et al.* 2008, 2009; Sims *et al.* 2008; Yang *et al.* 2012; Salama & Bett, 2014; Anneken *et al.* 2016). Oestrogen and progesterone interact acutely with multiple subcellular targets, altering the resultant emergent electrical activity at the level of cells and tissues (Nakamura *et al.* 2007; Yang *et al.* 2010; Kurokawa *et al.* 2015). During the menstrual follicular phase (prior to ovulation), oestrogen level is the highest, QT interval is longer and susceptibility to drug-induced arrhythmias is increased. In the luteal phase (following ovulation) progesterone is increased and arrhythmic events associated with acquired and

inherited long-QT syndrome are reduced (Burke *et al.* 1997; Rodriguez *et al.* 2001; Nakagawa *et al.* 2006; Anneken *et al.* 2016).

The differences in arrhythmia vulnerability during discrete stages of the menstrual cycle are likely to reflect the effects that sex steroid hormones have on cardiac ion channels (Kurokawa *et al.* 2008; Kurokawa *et al.* 2009). Oestradiol (E2) has been shown to inhibit I_{Kr}, although the specific interaction sites have not been fully identified (Kurokawa *et al.* 2008). The result of E2 interaction with hERG is an increase in ventricular action potential duration, consistent with the longer QT interval observed in women during the follicular phase of the menstrual cycle. Progesterone, on the other hand, enhances the slow delayed rectifier K$^+$ current (I_{Ks}), generated by the KvLQT1 channel (encoded by the *KCNQ1* gene), through a nitric oxide-dependent signalling pathway. This causes a decrease in ventricular action potential duration, consistent with the shorter QT interval observed during the luteal phase prolongation (Nakagawa *et al.* 2006). The effect of progesterone is similar to the effect of the male sex hormone testosterone, which not only enhances I_{Ks} via a NO-dependent mechanism, but also inhibits the inward Ca^{2+} current (I_{Ca-L}), both of which contribute to a shortening of the ventricular action potential and the QT interval in males after puberty (Bai *et al.* 2005).

There are also sex-based differences in the effects of the autonomic nervous system. Increased sympathetic or decreased parasympathetic stimulation produces a rate-dependent decrease in ventricular action potential duration (APD), but this effect is greater in men than in women (Magnano *et al.* 2002; Nakagawa *et al.* 2005; Hoeker *et al.* 2014). This correlates with a longer rate-corrected QT (QTc) interval in women. Changes in the balance of sympathetic and parasympathetic tone contribute to many types of arrhythmias often resulting in sudden cardiac death (Lanfranchi *et al.* 2010).

Long-QT syndrome type 2 patients are susceptible to sudden arousal associated with loud noise or emotional

Table 1. Experimental data for effects of testosterone on $I_{Ca,L}$ for males

Isoproterenol	I_{max} (pA pF^{-1})	$V_{1/2}$ (mV)	K	n
Activation				
ISO		$-24.7 + 1.9$	$4.9 + 0.5$	5
ISO + 100 nм DHT		-19.7 ± 2.1	5.3 ± 0.7	
Inactivation				
ISO	-27.0 ± 3.6	-26.8 ± 0.6	6.3 ± 0.3	7
ISO + 100 nм DHT	-19.9 ± 4.5	-28.9 ± 0.7	6.0 ± 0.2	

stress (Moss *et al.* 1999; Wilde *et al.* 1999). A recent population study noted that 82% of the observed arousal-induced arrhythmias occurred in females (Kim *et al.* 2010). In order to begin to understand why changes in autonomic tone are more likely to contribute to arousal-induced arrhythmias in females, we utilized computer models from our previous work that were based on and validated by experimental data to reflect acute actions of physiologically relevant human concentrations of sex steroid hormones progesterone, oestrogen and testosterone (Nakamura *et al.* 2007; Yang *et al.* 2010; Yang & Clancy, 2012). Here, we extended and expanded those models, and undertook simulations to reveal the conditions (i.e. pacing, drugs, sympathetic stimulation) required for triggering and sustaining reentrant arrhythmias in females in the setting of acute sympathetic arousal. We also employed a protein structure-based molecular docking approach to explore the possible interactions between oestrogen, hERG mutations and hERG blocking drugs like dofetilide. Like the hERG blocker ibutilide, which exhibits clear sex- and menstrual cycle-dependent effects (Rodriguez *et al.* 2001), Pham & Rosen (2002) reported that submicromolar concentrations of dofetilide coupled with physiological oestrogen levels produced a substantial APD$_{90}$ increase in females compared to males.

The results of this study suggest that specific therapeutic anti-arrhythmic strategies for women with long-QT syndrome should be studied. The study also suggests molecular determinants of drugs that might be especially problematic in females. These predictions might inform future drug design and screening.

Methods

Ethics approval

For Fig. 1 and Tables 1 and 2, experimental methods have been reported following the MICEE reporting standard (see www.micee.org): type: isolated cardiac ventricular myocytes; sex: male; weight: 251–350 g; species: Hartley guinea pig; supplier: Saitama Experimental Animal Supply Co. Ltd (Saitama, Japan).

Isolation procedure. Adult guinea pigs (white Hartley; 251–350 g) were deeply anaesthetized with intra-peritoneal injection of sodium pentobarbital (50 mg g^{-1},
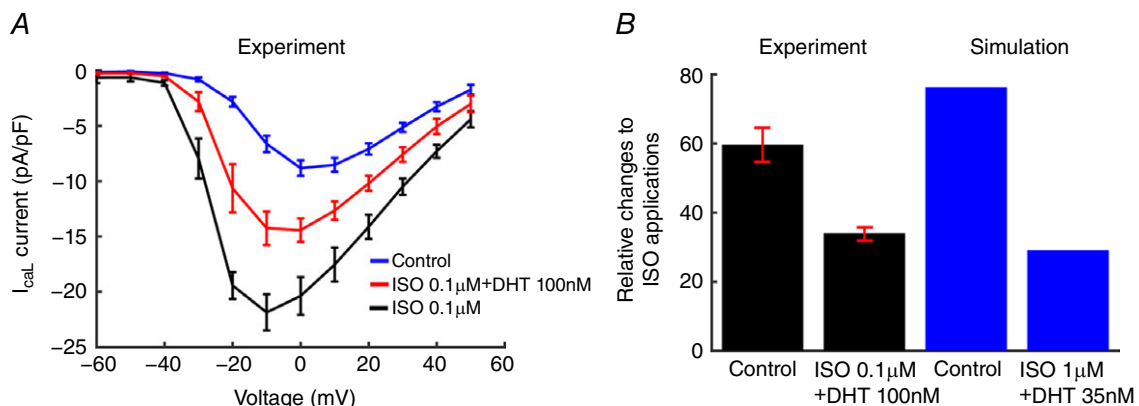
Figure 1. Simulated and experimentally recorded I_{caL} data under ISO stimulations
A, effect of DHT (100 nм) on *I–V* curves from guinea pig ventricular myocytes ($n = 5$). *B*, experimental data (error bars indicated by red, $n = 5$ for each case) compared to simulated relative changes of the peak I_{CaL} to ISO application.

Table 2. Experimental data for effects of DHT with cAMP + OA on $I_{Ca,L}$ current amplitude

	Normalized peak I_{CaL}		
DHT concentration	Mean (%)	SEM	*n*
100 nM	85.6	2.2	4
30 nM	81.3	10.6	2
10 nM	86.7	8.3	4
1 nM	98.8		1

Table 3. The female hormone concentrations used in the computational model

Menstrual cycle	17β-Oestradiol	Progesterone
Early follicular stage	0.1 nM	2.5 nM
Late follicular stage	1.0 nM	2.5 nM
Luteal stage	0.7 nM	40.6 nM

I.P.), and then killed by cervical dislocation. Hearts were perfused via the aorta with warm (36 ± 1°C) and oxygenated solutions as follows: (1) Tyrode solution containing (in mmol l^{-1}): 135 NaCl, 5.4 KCl, 1.8 CaCl$_2$, 1 MgCl$_2$, 10 glucose and 10 Hepes, pH 7.4, for 5 min; (2) Ca^{2+}-free Tyrode solution removing CaCl$_2$ from the Tyrode solution; (3) Ca^{2+}-free Tyrode solution containing collagenase (120 units ml^{-1}) and albumin (1 mg ml^{-1}), for 18 min; and (4) low-Ca^{2+} Tyrode solution with 0.2 mmol l^{-1} CaCl$_2$, for 5 min. At the end of the perfusion, the ventricles were minced in No. 4 solution to release single cells. Only the quiescent myocytes with clear striations were used for this study.

Electrophysiological recordings. For Fig. 1. L-type Ca^{2+} channel currents ($I_{Ca,L}$) were recorded with the whole-cell configuration of the patch-clamp technique with an Axopatch 200B amplifier (Molecular Devices, Sunnyvale, CA, USA). Signals were low-pass filtered at 5 kHz, sampled at 5 kHz, and compensated for cell capacitance (no series resistance compensation). The pCLAMP software (version 9.0, Molecular Devices) was used to generate voltage-pulse protocols, and for acquisition and analysis of data. The series resistance was 7.2 ± 0.6 MΩ, the capacitance time constant was 2.2 ± 0.3 ms, and the membrane capacitance was 139.3 ± 7.4 pF (*n* = 22). All experiments were performed at 36 ± 1°C. Pipette solution contained (in mmol l^{-1}): 130 CsCl, 2 MgCl$_2$, 5 adenosine-5′-triphosphate disodium salt, 10 Hepes, 20 TEA-Cl, 10 EGTA (pH 7.25 adjusted with CsOH). External (bath) solution contained (in mmol l^{-1}): 135 NaCl, 5.4 CsCl, 0.53 MgCl$_2$, 2 CaCl$_2$, 5.5 glucose and 5 Hepes (pH 7.4 adjusted with CsOH).

Effects of dihydrotestosterone (DHT) were obtained under sympathetic nervous system (SNS) activation by 10 min dialysis of 3′,5′-cyclic adenosine monophosphate (cAMP; 0.2 mmol l^{-1}) and okadaic acid (OA; 0.2 μmol l^{-1}) or by 3 min external application of (−)-isoproterenol (ISO) hydrochloride (0.1 μmol l^{-1}).

To monitor peak inward $I_{Ca,L}$, a pre-pulse (100 ms) was applied to –40 mV from a V_h of –80 mV to inactivate the Na$^+$ channels and the T-type Ca^{2+} channels, followed by a 200 ms V_t change to 0 mV at 1 Hz. To obtain

I–V relationships for measurement of $I_{Ca,L}$ activation, V_t was changed from −60 mV to 50 mV in 10 mV increments. To generate steady state inactivation curves, long pre-pulses (500 ms) to different voltages (−50 to 20 mV) were applied to allow inactivation to reach a steady state. Then the voltage was set to −40 mV for 10 ms to close the channels, after which a V_t change to 10 mV for 200 ms was applied to assess the state of inactivation of the channels.

Model development. We recently developed 'male' and 'female' computational model representations of human ventricular cardiac myocytes that include genomic-based differences in expression of key cardiac channels with human physiological concentrations of sex hormones on human action potentials (O'Hara *et al.* 2011; Yang & Clancy, 2012). The genomic differences were based on measured expression levels of key cardiac ion channel genes as well as connexin43 (underlying the dominant gap-junction subunit) in epicardial and end-ocardial ventricular tissue from non-diseased explanted male and female human hearts (Gaborit *et al.* 2010). We utilized these data (in construction of 'male' and 'female' human heart cell computational models by scaling the conductances of the corresponding currents in the O'Hara–Rudy human ventricular cell model (O'Hara *et al.* 2011) as described in Yang & Clancy (2012) (see also Appendix Table A1). Included in the male model based on new data (shown in Tables 1 and 2 and Fig. 1) is the effect of the acute application of a physiological concentration of testosterone (dihydrotestosterone, DHT) 35 nM, reflecting normal high ranges in post-pubescent pre-senescent males (Dorgan *et al.* 2002).

Simulation of acute sex steroid hormone effects

Three distinct female models were developed that include the hormones 17β-oestradiol (E2) (Munro *et al.* 1991; Dighe *et al.* 2005) and progesterone (Pg) (Munro *et al.* 1991; Janse de Jonge *et al.* 2001) during the early follicular, late follicular and luteal phases of the menstrual cycle. The hormone concentrations used in the model simulations and their specific sources are as shown in Table 3.

The E2 reference ranges are from Munro *et al.* (1991) and Dighe *et al.* (2005). The Pg reference ranges (used in

Table 4. G604S mutant values

	WT	Mutation
G_{Kr}	0.046	0.0147
R_{kr}	$1.0/\{1.0 + \exp[(v + 55.0)/75.0]\} \times 1.0/\{1.0 + \exp[(v - 10.0)/30.0]\}$	$1.0/\{1.0 + \exp[(v + 55.0 + 9)/75.0]\} \times 1.0/\{1.0 + \exp[(v - 10.0)/30.0]\}$
Reference	O'Hara *et al.* (2011)	Huo *et al.* (2008)

v is membrane potential (mV).

our initial study; Nakamura *et al.* 2007) are from Janse de Jonge *et al.* (2001) and Munro *et al.* (1991).

Simulating the effects of dofetilide

An I_{Kr} Markov model (Romero *et al.* 2014) was incorporated into the O'Hara–Rudy human ventricular action potential (AP) model (O'Hara *et al.* 2011) to simulate the effects of dofetilide on I_{Kr}.

Simulated G604S mutation

Experiments suggest that the G604S hERG pore loop mutation alters the current amplitude and the gating of the wild-type (WT) hERG channel. We simulated the mutant I_{Kr} (heterozygous channel: 50% each of WT and G604S) by modifying the conductance of WT current and also the kinetics of WT channel from the O'Hara–Rudy human model (O'Hara *et al.* 2011) based on the experimental data shown in Table 4.

Simulation of sympathetic nervous system: protein kinase A effects

We simulated the effects of 1 μM ISO on I_{caL}, I_{ks}, I_{kb}, I_{Na}, J_{rel}, J_{up}, troponin and I_{Nak}, according to O'Hara & Rudy (2012). In addition, progesterone and testosterone affect the conductance of I_{Ks}, but have no distinguishable effects on its kinetics under SNS stimulations. To model the effects of progesterone and testosterone on I_{Ks}, we modified G_{Ks} by scaling factors as indicated by the experimental data. In order to not overestimate the combined effects of DHT and SNS on I_{Ks}, we assumed that the combined effects reached a saturating level that is less than an additive effect, as was shown for progesterone. If the combination were additive, we would expect even more protection by testosterone in the setting of SNS.

Testosterone and SNS stimulation effects on I_{Ks}, I_{CaL} and the kinetics of the latter are shown in Table 5. DHT application during SNS stimulation affects the kinetics of $I_{Ca,L}$: the activation curve is less steep and is shifted to depolarized potentials compared to baseline (half-maximal activation shifted $\Delta V_{1/2} = 5$ mV and slope factor $\Delta k = 0.4$ for DHT 100 nmol l^{-1}). The inactivation curve is shifted in the hyperpolarized

direction and becomes steeper compared to baseline (half-maximal inactivation shifted $\Delta V_{1/2} = -2.1$ mV and slope factor $\Delta k = -0.3$).

In the simulations, we shifted the $I_{Ca,L}$ activation and inactivation curves by the same amount as above experimental data suggested to account for the different dosages of progesterone (see Table A2). Also the experimentally observed $I_{Ca,L}$ current reduction factor is 0.82 for [DHT] = 35 nM (Table 5). We used experimental data from 100 nM of DHT because 35 nM is a maximally stimulating dose of DHT on $I_{Ca,L}$ (Table 5). We then multiplied the scaling factors for I_{Ks} and $I_{Ca,L}$ when DHT is applied (see Table 5). Simulated results are in good agreement with experimental data shown in Fig. 1. The effects of progesterone on $I_{Ca,L}$ and I_{Ks} are shown in Appendix Table A2. Note that the ISO dose (0.1 μM) used in the experiments is a maximally stimulating dose.

Pacing protocol for arousal arrhythmia conditions

Cells were paced for 400 beats at basic cycle length (BCL) 1200 ms with no protein kinase A (PKA) effects, and followed by 10 beats (BCL = 800 ms) with PKA application.

Transmural tissue simulations

We simulated a transmural fibre composed of 360 ventricular cells ($\Delta x = \Delta y = 100$ μm) connected by resistances to simulate gap junctions (Faber & Rudy, 2000). The fibre contains an endocardial region (cells 1–160) and epicardial region (cells 161–360), with a linear decrease in APD as indicated by experimental data (Glukhov *et al.* 2010; Lou *et al.* 2011). G_{Kr} was used as the index value of endocardium in cell no. 1, and the index value of epicardium in cell no. 360. In the female model, G_{Kr} was monotonically increased from 0.036 to 0.042. In the male model, G_{Kr} was linearly increased from 0.046 to 0.05. AP simulations were carried out in epi-/endocardial cells by changing various ion channel conductances and gap-junctions (Yang & Clancy, 2012). The fibre was paced at BCL = 1200 ms for 500 beats and simulated arousal arrhythmia conditions (see above).

We simulated a heterogeneous 2D cardiac tissue composed of 360 by 440 cells with $\Delta x = \Delta y = 150$ μm. The tissue contains an endocardial region (fibres 1–160) and epicardial region (fibres 161–360). Channel conductance and gap-junction parameters are the same as in the one-dimensional simulations. Current flow is described by the following equation:

$$\frac{\partial V(x, y, t)}{\partial t} = D_x \frac{\partial^2 V(x, y, t)}{\partial x^2} + D_y \frac{\partial^2 V(x, y, t)}{\partial y^2}$$
$$- \frac{I_{ion} - I_{stim}}{C_m}$$

Table 5. Simulated effects of testosterone (DHT) on I_{Ks} and $I_{Ca,L}$

Channel	DHT		DHT (SNS stimulation)
	10 nM	35 nM	35 nM
I_{Ks}	1.38	1.4	3.52
I_{CaL}	0.94	0.82	2.05
Kinetics of I_{CaL}	No effects		$d_{ss} = 1.0/\{1.0 + \exp[(-(v + 3.94 + 16 - 5.0))/4.63]\}$
			$f_{ss} = 1.0/\{1.0 + \exp[(v + 19.58 + 8.0 + 2.1)/3.396]\}$
Reference	Bai *et al.* (2005)		Table 1

v is membrane potential (mV).

where V is the membrane potential, x and y are distances in the longitudinal and transverse directions, respectively, D_x and D_y are diffusion coefficients in the x and y directions, C_m is membrane capacitance ($C_m = 1$), and I_{stim} is 180 mA cm^{-2} for the first 0.5 ms. We also incorporated anisotropic effects by setting D_x and D_y such that the ratio of conduction velocities is 1:2 (Young & Panfilov, 2010).

The tissue was first paced for 500 beats at BCL = 1000 ms on the entire length of one side of tissue prior to application of SNS, and then the 501th beat was paced on the top left corner in an endocardial region with no PKA effects at BCL = 1000 ms followed by PKA additions in the next beat paced in the same region.

Pseudo-ECG computation. Extracellular unipolar potentials (Φ_e) generated by the fibre in an extensive medium of conductivity σ_e, were computed from the transmembrane potential V_m using the integral expression as in Gima & Rudy (2002).

In one dimension:

$$\Phi_e(x') = \frac{a^2 \sigma_i}{4\sigma_e} \int (-\nabla V_m) \bullet \left[\nabla \frac{1}{r} \right] dx$$

$$r = [(x - x')^2]^{1/2}$$

In two dimensions:

$$\Phi_e(x', y') = \frac{a^2 \sigma_i}{4\sigma_e} \int (-\nabla V_m) \bullet \left[\nabla \frac{1}{r} \right] dx dy$$

$$r = [(x - x')^2 + (y - y')^2]^{1/2}$$

where ∇V is the spatial gradient of V_m, a is the radius of the fibre, σ_i is the intracellular conductivity, σ_e is the extracellular conductivity, and r is the distance from a source point (x, y) to a field point (x', y'). Φ_e was computed at an 'electrode' site 2.0 cm away from the distal end along the fibre axis.

Action potential duration mapping. We reconstructed 'human transmural myocardial' based on data describing transmural action potential heterogeneity mapped from normal human left ventricle (Glukhov *et al.* 2010) (Fig. 8A). First, the O'Hara–Rudy human model was used

to generate a G_{Kr} lookup table corresponding to APD$_{80}$. Next, an experimental 2D APD$_{80}$ map (100×100–Fig. 8A) was used to create a 2D G_{Kr} map using the G_{Kr} lookup table. Then the two-dimensional G_{Kr} values (100×100) were used to simulate APD$_{80}$. We paced the female heart at 1 Hz and modified the length of APD$_{80}$ to match the clinically observed QT intervals $\sim$400 ms (Stramba-Badiale *et al.* 1997; Ebert *et al.* 1998; Nakagawa *et al.* 2005). We then constructed a 3D wedge of 100 by 100 by 1 with $\Delta x = \Delta y = 200$ μm and $\Delta z = 500$ μm using this APD mapping data. Current flow is described by the following equation:

$$\frac{\partial V(x, y, z, t)}{\partial t} = D_x \frac{\partial^2 V(x, y, z, t)}{\partial x^2} + D_y \frac{\partial^2 V(x, y, z, t)}{\partial y^2}$$
$$+ D_z \frac{\partial^2 V(x, y, z, t)}{\partial z^2} + -\frac{I_{ion} - I_{stim}}{C_m}$$

where V is the membrane potential, D_x, D_y and D_z are diffusion coefficients in the x, y and z directions, and I_{stim} is 150 mA cm^{-2} for 0.5 ms. We also incorporated anisotropic effects by setting D_x, D_y and D_z such that the ratio of conduction velocities is 2:4:1 (Young & Panfilov, 2010).

Structural model development

The SWISS-MODEL homology modelling program (Kopp & Schwede, 2004) was used for the development of the hERG model from the available Eag1 channel cryo-EM structure (PDB ID 5K7L), determined at 3.78 Å resolution (Model 1). A multiple sequence alignment was performed using the CLUSTALW algorithm (Thompson *et al.* 1994). Protein models were generated from the alignment in a stepwise manner. The conserved backbone coordinates of the template were preserved in the final model (Wang *et al.* 2016). The gap regions in the sequence alignment were modelled either from a loop library or through a conformational space search using constrained element methods. The scoring function used for determining side chain conformations was derived from a backbone-dependent rotamer library (Benkert *et al.* 2011) that accounts for favourable interactions,

such as hydrogen bonds and disulfide bridges, as well as unfavourable close contacts. A more detailed description of protocols and sequence alignments used for hERG model generation were provided previously (Durdagi *et al.* 2012; Anwar-Mohamed *et al.* 2014; Wang *et al.* 2016).

Model 1 was used to study all interactions between E2 and extracellular pore loop residues in both WT and G604S mutant. While this model provides a new template for understanding the effects of mutations in this region, it contains a pore domain in the closed state, and the molecular volume available for binding inside the pore is far too small to accommodate any of the common blockers. Therefore, to study the potential interactions between the channel and hERG blockers, we used a previously developed and experimentally validated model of the hERG pore in the open state (Durdagi *et al.* 2012; Anwar-Mohamed *et al.* 2014) based on the Kv1.2 X-ray crystal structure (PDB ID 2A79), determined at 2.9 Å resolution (Model 2). It is important to stress that this previously published model of the hERG pore displays remarkable structural conservation with the published Eag1 structure for residues critical for drug binding (T623, S624, Y652 and F656), with major differences in the pore loop region far away from the common intra-cavity binding site (Wang *et al.* 2016). To further refine both Model 1 and Model 2 of the hERG channel, we performed molecular dynamics (MD) simulations with a protocol described below.

Molecular docking and MD simulations

First, the molecular structure of oestradiol (E2) was downloaded from the ZINC database (Irwin *et al.* 2012) and the partial charges were recalculated using the GAAMP protocol (Huang & Roux, 2013). Next, molecular docking was performed using the Glide-XP (extra precision) and Induced Fit Docking (IFD) modules of the Maestro suite from Schrödinger (Gabrielsen *et al.* 2012) for dofetilide and E2 binding to Model 1 and Model 2. A molecular grid of 36 Å × 36 Å × 36 Å was used to map binding pockets on the hERG surface. We followed the recommended protocol for docking of dofetilide and oestradiol including the following steps: (1) constrained minimization of the receptor with a root mean square deviation cutoff of 0.18 Å; (2) initial Glide docking of each ligand using soft potentials; (3) refinement of the derived docking poses (i.e. minimization of the protein receptor site within 20 Å of the ligand-bound area) with Schrodinger's Prime module; and (4) Glide re-docking of the protein–ligand complexes. Clustering analysis was used to evaluate the docking poses in both the poor loop (using Model 1), and intracellular cavity site (using Model 2). The top-scoring pose from each docking simulation was used for MD simulations. We considered five hERG–substrate complexes in total, including hERG–E2 (pore loop WT), hERG–E2 (pore loop G604S), hERG–E2 (cavity), hERG–dofetilide (cavity), and hERG–E2–dofetilide (cavity). CHARMM-GUI (Jo *et al.* 2008) was used to prepare protein–dipalmitoylphosphatidylcholine lipid bilayer complexes solvated in 150 mM KCl aqueous solution using CHARMM-36 force field and TIP3P water model (Jorgensen *et al.* 1983; MacKerell *et al.* 1998; Noskov *et al.* 2004; Noskov & Roux, 2008; Klauda *et al.* 2010; Best *et al.* 2012). The remaining parameters for oestradiol were generated with MATCH (Yesselman *et al.* 2012). The molecular parameters for a neutral form of dofetilide were reported previously (Wang *et al.* 2016). The fully assembled systems were equilibrated for 10 ns using NAMD2.10 (Phillips *et al.* 2005), and production runs were then performed for 50 ns for E2 binding to the WT and G604S mutant pore loop site (Model 1). Both dofetilide and E2 binding to the intracellular cavity (Model 2) were studied with 100 ns MD simulations. All production runs were performed under a constant temperature and pressure (*NPT*) ensemble, with a pressure of 1 atm and temperature of 315.15 K. Long-range electrostatic interactions were treated by the particle mesh Ewald (PME) algorithm (Essmann *et al.* 1995). Non-bonded interactions were switched off at 10–12 Å. The systems were simulated with a time step of 2 fs under periodic orthorhombic boundary conditions. The ensembles of frames obtained from various MD simulations were used for the calculation of binding enthalpies using a previously developed protocol based on continuum solvent model enthalpies (Robertson *et al.* 2008).

Results

Combined effects of sex, SNS and I_{Kr} channel blocking drugs

Clinical and experimental studies have shown that females are especially susceptible to QT-interval prolongation by I_{Kr} blocking drugs (Kurokawa *et al.* 2008). This finding may partially explain why females are more prone to drug-induced arrhythmias (Makkar *et al.* 1993; Lehmann *et al.* 1996). Hence, we tested the combined effects of hormones and the I_{Kr} channel blocker dofetilide on SNS-induced arrhythmia triggers.

Dofetilide is a prototype of the pro-arrhythmic class – associated with hERG block, QT prolongation and TdP (Van Opstal *et al.* 2001). We recently developed a detailed kinetically based model of the hERG blocker dofetilde by extending the consensus five-state Markov chain model that includes three closed states (C_3, C_2 and C_1), a conducting open state (O) and an inactivation state (I) (Romero *et al.* 2014). The expanded I_{Kr} model that includes dofetilide interactions was incorporated into the O'Hara–Rudy model of the

human ventricular action potential (AP) (O'Hara *et al.* 2011).

The dofetilide model, described and validated in detail previously (Romero *et al.* 2014), includes the experimentally observed 70-fold preferential binding to the inactivated state relative to the open state (Perrin *et al.* 2008) and mimics the clinically observed 16% prolongation of the QT interval produced by the therapeutic dose 8.22 nM (Demolis *et al.* 1996). The effects of the female hormones 17β-oestradiol (E2) and progesterone (Pg), the male hormone dihydrotestosterone (DHT) and sex-specific genomic-based differences in expression of key cardiac channels on human action potentials from this study and O'Hara *et al.* (2011) and Yang & Clancy (2012) were also incorporated to develop female and male models as described in more details in Methods above.

We utilized these male and female models and added the combined effects of dofetilide with acute effects of β-adrenergic stimulation by isoproterenol to predict the combined effects of (1) genomic-based differences in expression of key cardiac channels, (2) human physiological concentrations of sex hormones, (3) an inherited long-QT syndrome and (4) sympathetic arousal that includes an increase in pacing rate.

Simulation of cell-level effects of sex-based arousal arrhythmias

Figure 2 (upper panels) shows the predicted effects of dofetilide to generate arrhythmia triggers in single simulated myocytes in the early follicular phase of the menstrual cycle (Fig. 2*A*), the late follicular phase (Fig. 2*B*), the luteal phase (Fig. 2*C*) and in the presence of testosterone (Fig. 2*D*). Shown are the predicted effects of sex differences and SNS in the setting of acquired long-QT syndrome, modelled as the application of dofetilide. Action potentials are shown following pacing for 400 paced beats at a cycle length of 1200 ms in single simulated endocardial cells. The 399th and 400th paced beats are shown, after which SNS was acutely applied and the pacing cycle length increased to 800 ms to mimic SNS effects on heart rate. Upon acute SNS application arrhythmia triggers were observed in single myocytes (upper panels) in both the early follicular phase of the menstrual cycle (Fig. 2*A*) and in the late follicular phase (Fig. 2*B*). The follicular phases of the menstrual cycle when oestradiol is highest were especially vulnerable. Progesterone was apparently protective during the luteal phase (Fig. 2*C*) as was the presence of testosterone (Fig. 2*D*). These simulations predict that the female cardiac myocytes in the presence of a hERG blocker exhibit arrhythmogenic rhythms upon SNS. When no drug or SNS was applied, no arrhythmogenic rhythms were observed (Appendix Fig. A1).

Simulation of tissue-level effects of sex-based arousal arrhythmias

We also explored the effects of sex-based differences in the setting of acquired long-QT syndrome type 2 and acute SNS in a one-dimensional transmural strand of coupled cells comprising epicardial to endocardial regions (detailed explanation of construction of the tissue is in Methods).

Figure 2 (middle and lower panels) illustrates the predicted sex differences in tissue arrhythmia vulnerability during acquired long-QT following arousal by SNS. Simulations in one-dimensional transmural tissue composed of coupled cells (360 cells) are shown in the presence of 10 nM dofetilide during the early follicular phase of the menstrual cycle (Fig. 2*A*). Time is shown on the *x*-axis and voltage on the *z*-axis in the middle panels. The corresponding electrograms are shown in each panel below the space-time plots. Simulated action potentials (APs) are shown following pacing for 400 beats at 1200 ms pacing cycle length. The last 3 beats are shown and then SNS was acutely applied and the cycle length was increased to 800 ms. As shown in Fig. 2*B*, the late follicular phases of the menstrual cycle where oestradiol is highest exhibits an arrhythmogenic rhythm triggered by the acute application of SNS. An early afterdepolarization (EAD) initiated in the endocardial region (in the late follicular case shown in Fig. 2*B*) generates a sufficient source current to drive full action potential initiation in the downstream excitable (repolarized) epicardial region. The second depolarization during the endocardial EAD results in a self-sustaining oscillation derived from a spatially discordant alternans that zig-zags back and forth to re-excite downstream or upstream cells. The excitatory signal is runaway, as it is a self-generating oscillation in the form of a one-dimensional reentry. Both an increase in progesterone during the luteal phase (Fig. 2*C*) and testosterone in the male tissue (Fig. 2*D*) were predicted to protect against SNS arrhythmia provocation.

We next tested the vulnerability to arrhythmia induced by SNS in models of acquired long-QT syndrome in simulated human male and female two-dimensional tissues as shown in Fig. 3 by simulating a heterogeneous cardiac tissue containing an endocardial region (tissue columns 1 to 160) and an epicardial region (tissue columns 161 to 360) based on recordings from human tissue (Glukhov *et al.* 2010; Lou *et al.* 2011) also incorporating anisotropic effects as described in detail in Methods above. Following pacing for 500 beats (s1) at BCL = 1000 ms along the entire endocardial length, SNS was then applied with an additional stimulus (s2) after which the simulation ran for 3000 ms without any additional stimulation.

Figure 3 shows voltage snapshots in time as indicated prior to and following the application of SNS in two-dimensional tissue models. The simulated male tissue
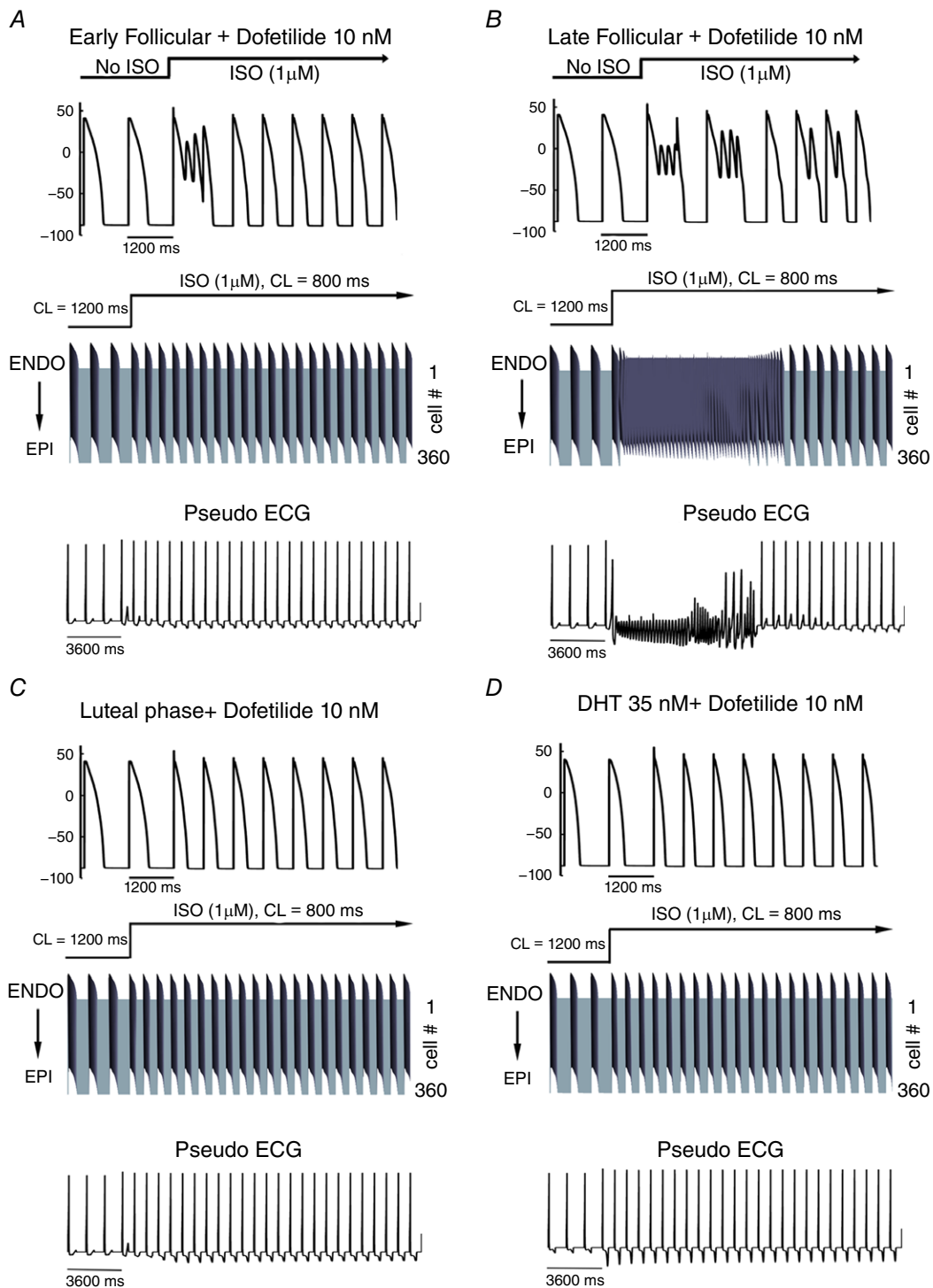
Figure 2. Sex-based differences in human cardiac electrophysiology predicted in the setting of acquired long-QT syndrome induced by dofetilide

Single cell action potentials were simulated before and during simulated arousal via sympathetic stimulation following pretreatment with dofetilide (top panel *A–D*). Transmural 1-dimensional tissue models and pseudo-ECGs were simulated before and during SNS. The pseudo ECG is shown beneath the tissue simulation in each panel. *A*, simulated combined effects of oestradiol and progesterone on female tissues during the early follicular phase of the menstrual cycle. *B*, simulated combined effects of oestradiol and progesterone on female tissues during the late follicular phase of the menstrual cycle. *C*, simulated combined effects of oestradiol and progesterone on female tissues during the luteal phase of the menstrual cycle. *D*, simulated effect of testosterone on male tissue during SNS.

with testosterone is shown in Fig. 3*D*. The 500th paced beat is shown prior to application of SNS. The presence of dofetilide resulted in SNS-induced self generated arrhythmias in the female simulated tissues during the early follicular (Fig. 3*A*) and late follicular (Fig. 3*B*) phases of the menstrual cycle. The time course of single cell action potentials from two points in space (labelled as 'a' and 'b') in the simulated 2D tissue and the computed electrograms are shown in the right columns. Site 'a' undergoes two consecutive stimuli (indicated as '1st and '2nd') at 10 ms and 1010 ms. Sympathetic activation occurs concurrently with the second stimulus. However, the site of activation (near 'a') becomes a site of reactivation via back-propagating action potential conducted from downstream tissue (near 'b'). The tissue near site 'a' then re-excites site 'b', which continues in a feedback loop (observed as an oscillation on the computed electrogram), during which site 'a' maintains depolarization and serves as a persistent current source.

When progesterone was high during the luteal phase (Fig. 3*C*), no arrhythmias were predicted. We also did not observe any arrhythmias in the male model when testosterone was present (Fig. 3*D*). Application of dofetilide led to development of spontaneous oscillations

in the female only – suggesting vulnerability to arrhythmia in the follicular phases of the menstrual cycle. The computed electrograms from the tissue in Fig. 3*A* and *B* exhibit both periodicity and sinusoidal amplitude, consistent with torsade de pointes type arrhythmias.

Simulation of structural molecular-level effects of sex-based arousal arrhythmias

The cellular- and tissue-level simulations discussed above suggest that cardiac ion channel hormone interactions may constitute an important component of sex-based arousal arrhythmias with I_{Kr} current modulation playing a central role. Experimentally the reduction of I_{Kr} resulting from the action of oestradiol on the hERG channel has been demonstrated previously (Kurokawa *et al.* 2008); however, the molecular-level interactions that underlie this effect remain uncharacterized. As a first step to identify potential binding sites as well as key stabilizing interactions between ligand and receptor, we carried out molecular docking of dofetilide (Fig. 4*A*) and E2 (Fig. 4*B*) to the intra-cellular cavity (IC) of the WT open-state hERG atomistic model (Model 2) developed previously (Durdagi *et al.* 2011, 2012).
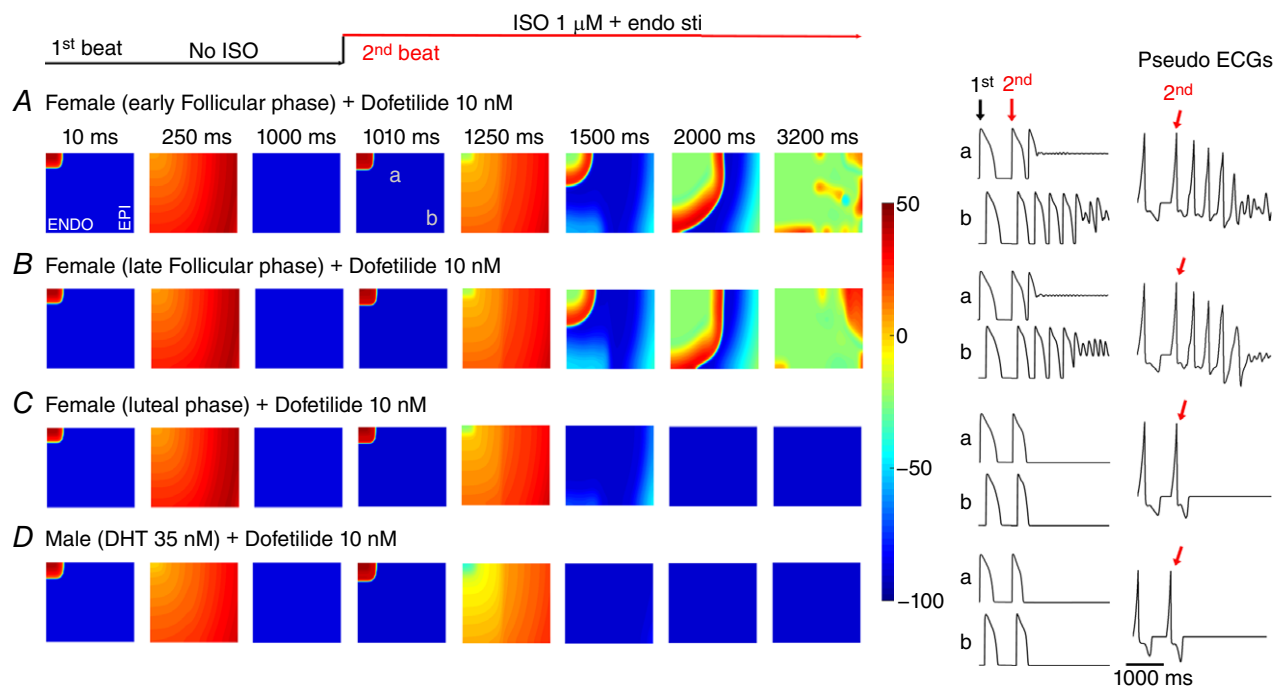

Figure 3. Female sex is predicted to increase susceptibility to reentrant arrhythmia following acute SNS stimulation in the setting of acquired long-QT syndrome induced by dofetilide application
A–B, predicted reentrant wave following SNS on female heterogeneous tissue (5.4 cm × 6.6 cm) containing an endocardial region (tissue columns 1–160) and an epicardial region (tissue columns 161–360) based on recordings from human tissue, and anisotropic conduction in the presence of female hormones during the early follicular (*A*), late follicular (*B*) and luteal phases (*C*) of the menstrual cycle. *D*, no arrhythmia was predicted in male tissue with 35 nM testosterone. Single APs from site 'a' and site 'b' in the simulated tissues are shown in the middle panels for each case. Computed electrograms from simulated tissues are shown in the right panels.
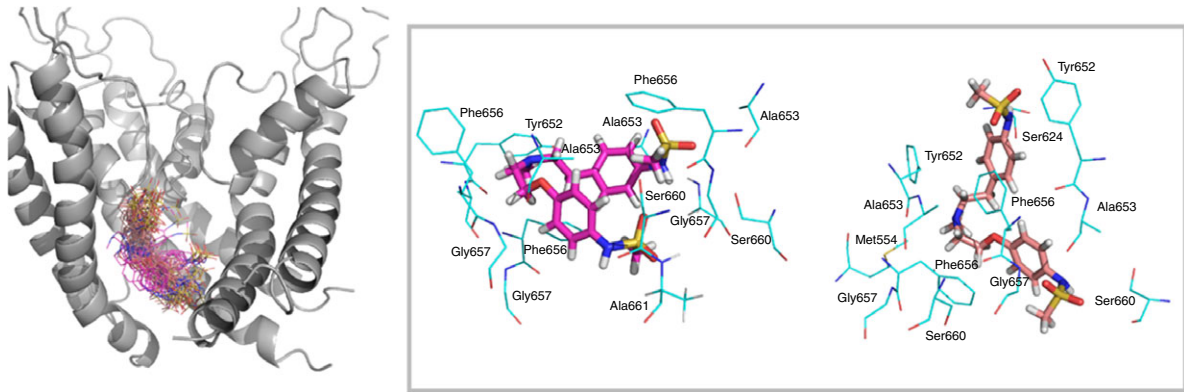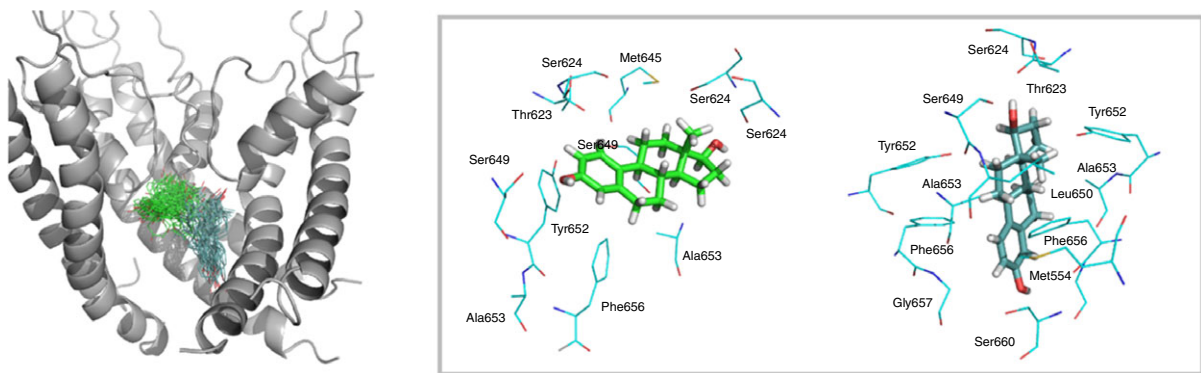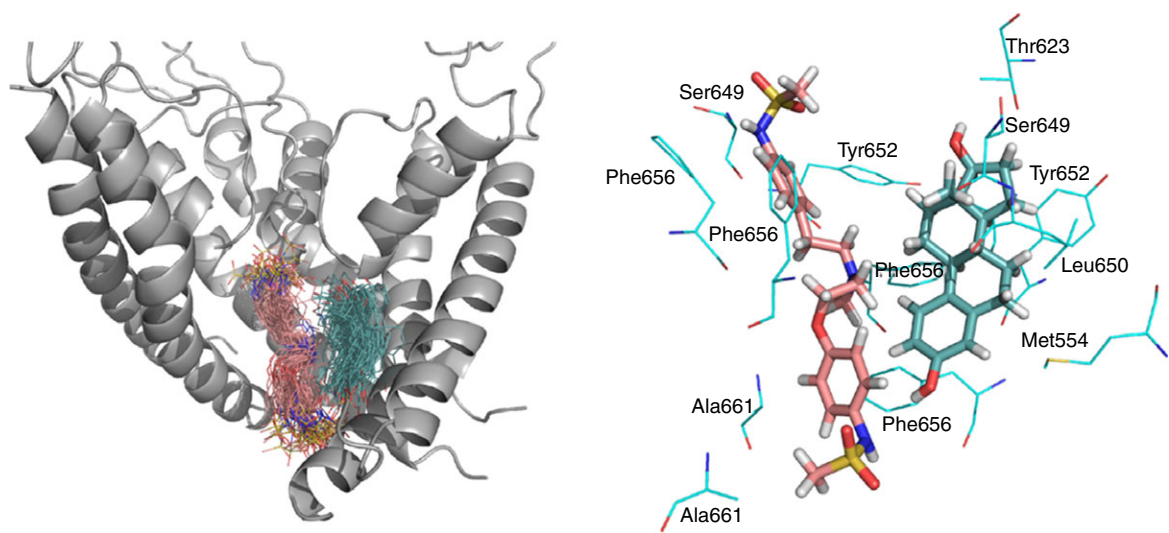
Figure 4. Top scoring docking poses for dofetilide (*A* and *C*) and oestradiol (*B* and *C*) in the intracellular cavity (IC) site of hERG
Left panels: pore domain of the hERG open state model and selected frames showing dofetilide (pink) (*A*), and E2 (green) (*B*), binding to the IC. Right panels: average position of dofetilide (*A*), and E2 (*B*) shown together with coordinating residues within 3.5 Å for two mapped binding sites. Two dominant binding orientations are shown in magenta and pink for dofetilide (*A*), and in green and light-blue for E2 (*B*). The relative orientation of dofetilide (pink) and E2 (light-blue), as well as the dominant interacting residues in the hERG IC site, are shown in *C*.

The simulations showed that a clustering of dofetilide poses that provides additional confirmation that dofetilide interacts with binding pocket for common hERG blockers (Fig. 4*A*; Vandenberg *et al.* 2001; Ficker *et al.* 2001; Durdagi *et al.* 2012). E2 poses and follow-up MD simulations led to identification of two tentative binding pockets with favourable binding docking scores for the oestradiol molecule. The high-affinity site, shown in Fig. 4*B*, is located in the intracellular cavity of hERG and overlaps with a binding pocket for common hERG blockers including dofetilide (as shown in Fig. 4*A*) (Durdagi *et al.* 2012). To provide in-depth analysis of E2 dynamics in this IC site, we performed 100 ns MD simulations of the hERG–E2 complex in explicit lipid bilayers. The oestradiol molecule exhibits substantial flexibility in the IC of hERG, resulting in a broad distribution of binding enthalpies. However, most of them are in the −10 to −15 kcal mol^{-1} range with a mean value around −12 kcal mol^{-1}, which (without taking into account entropic contribution) corresponds to low micromolar/potent blocking affinity (Zachariae *et al.* 2009; Anwar-Mohamed *et al.* 2014). Similar to many other blockers, oestradiol explores both low- and high-affinity sites in the IC of hERG channel (Duff *et al.* 1995; Lees-Miller *et al.* 2000). Analysis of MD simulations shows that the most dominant binding pocket for E2 relies on a combination of π-stacking interactions of Y652 and F656 rings with an aromatic centroid of E2, supplemented by hydrogen bonding with the constellation of T623/S624 in the pore helix region and S645 in the S6 helix.

The second binding site is defined by the aromatic F656 side-chain, supplemented by a number of hydrophobic residues including L650 and A653. Y652 is also transiently involved into coordination of bound oestradiol at this site. It is apparent that the main determinant of binding is whether the F656–E2 interaction can be stabilized by the additional hydrophobic interactions. Kurokawa *et al.* (2008) have shown that E2 does not inhibit both F656T and F656M mutant hERG currents, which is in agreement with the theoretical results presented here. It is notable that the relatively small size of oestradiol allows for another orientation in the binding pocket, where the bound hormone is oriented along the two distal S6 helices from adjacent subunits.

The E2 IC binding site is adjacent to that of dofetilide (see Fig. 4*C*), suggesting a likely interaction. In fact, our binding enthalpy calculations from MD simulations demonstrated that the presence of intracellular cavity bound E2 leads to a modestly more favourable binding of dofetilide (by around 1.2 kcal mol^{-1}). Also, the width of the distribution for dofetilide binding energies is much narrower with E2 bound to IC of hERG channel. All this suggests that a presence of E2 can potentially enhance hERG block by dofetilide, and thus enhance its proclivity to promote arrhythmia. The combination of molecular docking, MD simulations and binding enthalpy computations in conjunction with electrophysiology data provides consistent evidence for IC blocker action of E2.

Simulation of cellular-level effects of inherited sex-based arousal arrhythmias

We next extended the O'Hara–Rudy computational model (O'Hara *et al.* 2011) of I_{Kr} to include the functional effects of the cardiac pore loop mutation G604S. As shown in Fig. 5*A* and *B*, the mutant G604S I_{Kr} model was developed by optimizing parameters to experimental data for current–voltage relationships of peak and tail currents of G604S I_{Kr} recorded from HEK cells. In Fig. 5*A* and *B*, the adjusted, model-generated I_{Kr} (lines) is shown superimposed on experimental I_{Kr} records (symbols). The normalized I_{Kr} current–voltage relationship for
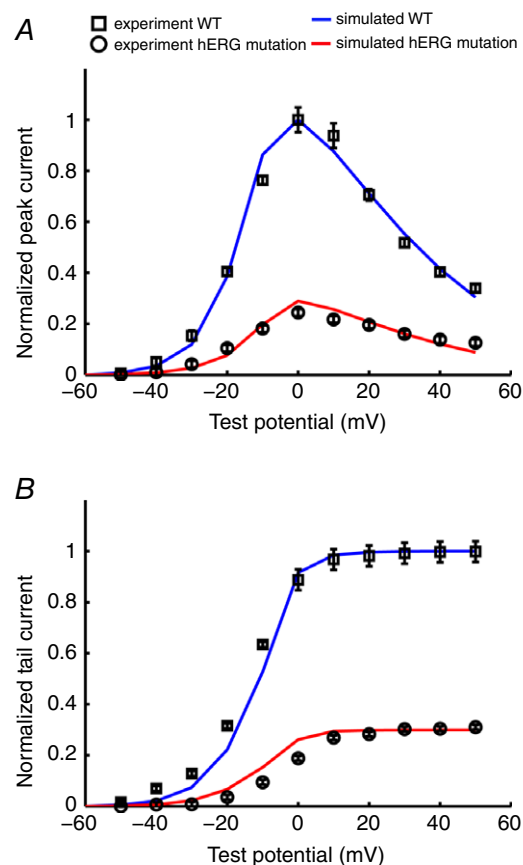

Figure 5. Simulated and experimentally recorded I_{Kr} data
Model-generated I_{Kr} (lines) is shown superimposed on experimental I_{Kr} records (symbols with error bars, $n = 9$) from HEK cells (Huo *et al.* 2008). *A*, normalized I_{Kr} current–voltage relationship for peak current for WT (blue) and the hERG-G604S mutation (red). *B*, current–voltage relationships from normalized tail currents for WT (blue) and hERG-G604S mutant channels (red).

peak current for WT (black) and the hERG-G604S mutation (red) are shown in panel (A). In panel (B) there are current–voltage relationships from normalized tail currents for WT (blue) and hERG-G604S mutant channels (red).

To determine the sex-based propensity for arousal-induced arrhythmias, we added the combined effects of the long-QT syndrome type 2 pore mutation G604S with acute effects of β-adrenergic stimulation by isoproterenol. Figure 6 shows the predicted effects on arrhythmia triggers in single simulated myocytes (upper rows) in female and male models. These results indicate that the female cells in the presence of the G604S pore mutation, particularly in the follicular phases of the menstrual cycle when oestradiol is highest, are considerably more vulnerable to the emergence of arrhythmogenic rhythms upon SNS.

Simulation of tissue-level effects of inherited sex-based arousal arrhythmias

We next explored the effects of sex-based differences in the setting of inherited long-QT syndrome type 2 pore mutation G604S and acute SNS in a one-dimensional transmural strand of coupled cells comprising epicardial to endocardial regions. The middle panels in Fig. 6A–C (middle rows) show the sex-based effects in an electrically coupled female tissue during the early follicular (Fig. 6A), late follicular (Fig. 6B) and luteal (Fig. 6C) phases of the menstrual cycle. The male tissue with testosterone present is shown in the middle of Fig. 6D. We also computed electrograms (lower panels) in female and male virtual tissues (Fig. 6).

Importantly, the simulation shows longer repolarization in the female compared to male tissues following SNS, consistent with the longstanding observations that females have longer corrected QT intervals than males (Jose & Collison, 1970; Huikuri *et al.* 1996; Burke *et al.* 1997; Stramba-Badiale *et al.* 1997; Bidoggia *et al.* 2000; Smetana *et al.* 2002). The prolonged T-wave in females corresponds to longer APD (as observed in the space–time plot) and is likely to contribute to the arrhythmogenic rhythm that emerges in the late follicular phase (Fig. 6B). Note that the computed electrogram from the tissue in Fig. 6B exhibits both periodicity and sinusoidal amplitude, consistent with torsade de pointes type arrhythmias.

We also tested the vulnerability to arrhythmia induced by SNS with the LQT2 G604S hERG pore mutation in simulated human male and female two-dimensional tissues using the same protocol as described in Fig. 3. Figure 7 shows voltage snapshots in time as indicated prior to and following the application of SNS in female tissue in simulated phases corresponding to early follicular (Fig. 7A), late follicular (Fig. 7B) and luteal (Fig. 7C) phases of the menstrual cycle. The simulated male tissue with testosterone is shown in Fig. 7D. Simulations are shown

following pacing from the endocardium for 500 beats at 1000 ms pacing cycle length. The 500th paced beat is shown prior to application of SNS. In the presence of testosterone (Fig. 7D) or high progesterone (luteal phase in Fig. 7C) application of SNS is not predicted to be arrhythmia provoking.

The outcome was starkly different in the female simulated tissue during the early (Fig. 7A) and late follicular (Fig. 7B) phases, which following SNS application developed spontaneous focal arrhythmia activity – in these cases, the oscillations persist for more than 3 s. The development of spontaneous sustained oscillations suggests female vulnerability to arrhythmia is especially noticeable during the follicular phases of the menstrual cycle. The computed electrograms from the simulated tissues are shown in the right panels, clearly illustrating the abrupt degeneration of the electrical rhythm following acute SNS in Fig. 7A and B. Notably, in the absence of either the G604S pore mutation or SNS, no arrhythmia was observed at the cell (Appendix Fig. A1) and tissue levels (Appendix Fig. A2).

Finally, because a three-dimensional tissue is a larger electrotonic sink, we set out to test if the predictions of female vulnerability to SNS-induced arrhythmia in the setting of long-QT syndrome type 2 would persist in higher dimensions. We developed an *in silico* left ventricular 3D wedge reconstruction of the human female based on the experimental data from Glukhov *et al.* (2010) with the pore loop G604S mutation (Fig. 8). Even in the 3D wedge reconstruction, we observed arousal-induced spontaneous arrhythmias in the early follicular (Fig. 8A) and late follicular (Fig. 8B) phases of menstrual cycle by acute SNS application. Just as in lower dimensions, the luteal phase is not predicted to be sensitive to SNS (Fig. 8C).

Ionic mechanisms of arrhythmia vulnerability in females

We next utilized a component dissection approach to determine the mechanism of self-generated arrhythmia triggers in the late follicular phase of the menstrual cycle. Because PKA activity results in increases in two inward currents, I_{Na} and I_{CaL}, it is difficult to assess which effect is required to promote arrhythmogenic early afterdepolarizations. Thus, we selectively blocked the individual effects of PKA facilitation of I_{Na} and I_{Ca}, while maintaining all other effects. The 399th–400th beats (red arrows) are shown prior to application of SNS. Upon SNS application, the pacing cycle length was increased to 800 ms for 100 beats. The last 11 of 100 beats (BCL = 800 ms, under SNS stimulations) are shown in the right panels. As can be seen in Fig. 9A–C, the blocking PKA effects on I_{CaL} alone was sufficient to prevent arrhythmia triggers, which did not emerge even after 100 beats (right
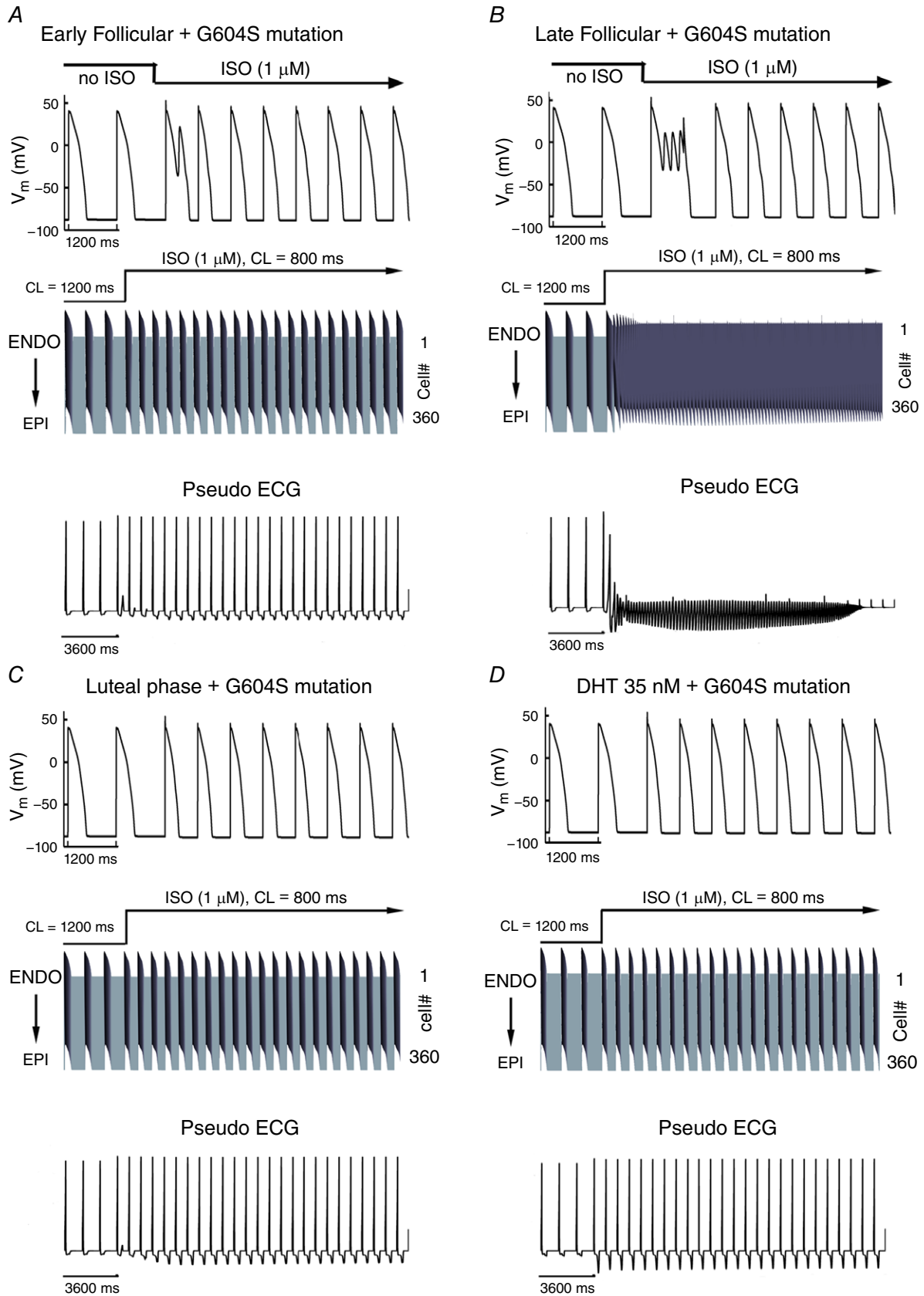
Figure 6. Simulated arousal via sympathetic stimulation in the setting of the G604S mutation causing inherited long-QT syndrome type 2

Single cell action potentials are shown at the top of each panel. Transmural 1-dimensional tissue models are shown in the middle. Time is shown on the *x*-axis and voltage on the *z*-axis. The pseudo ECG is shown beneath the tissue simulation in each panel. *A*, simulated combined effects of oestradiol and progesterone on female tissues during the early follicular phase of the menstrual cycle. *B*, simulated combined effects of oestradiol and progesterone on female tissues during the late follicular phase of the menstrual cycle. *C*, simulated combined effects of oestradiol and progesterone on female tissues during the luteal phase. *D*, simulated effect of testosterone on male tissue during SNS.

panels). On the other hand, blocking the effects of PKA on I_{Na} (Fig. 9*D–F*) did not prevent afterdepolarizations, which persisted after 100 additional beats (right panels). Finally, based on recent data from the Salama group, we examined the effect of increasing I_{NCX} (NCX is a sodium–calcium exchanger) density by 2-fold (Chen *et al.* 2011) in the epicaridum as shown in Fig. 9*G–I*. The cell (Fig. 9*G*, red line) and coupled tissue (Fig. 9*H*) exhibited an exacerbation of proarrhythmia when the I_{NCX} density was increased compared with no changes in I_{NCX} (black line). The effect on the computed electrogram is shown as a tachycardic rhythm in Fig. 9*I*.

The explanation for this mechanism can be traced back in part to the effects of hormones on the I_{CaL} window current. Progesterone and testosterone cause a dose-dependent reduction in I_{CaL} window current (Appendix Fig. A3). During the follicular phases of the menstrual cycle, low progesterone (2.5 nM) does not sufficiently reduce the I_{CaL} window current, which when combined with reduced hERG current due to long-QT syndrome type 2 mutations or drugs, resulted in increased susceptibility to EADs in female myocytes during the follicular phase. Our simulations suggest that EADs were initiated by a perfect storm of PKA effects, acute hormone effects on I_{CaL} and I_{Kr} suppression by the long-QT syndrome type 2 mutation or dofetilide (Appendix Fig. A4). At the tissue level, there is an additional effect in the female of reduced gap junction conductance, incorporated in our model based on the observation of reduced Cx43 in female *versus* male hearts (Gaborit *et al.* 2010; Yang & Clancy, 2012). Reduced gap junction coupling (Xie *et al.* 2010) in the female relative to male (Appendix Table A1) is predicted to promote the development of EADs, by creating a source–sink mismatch that allows for triggered activity in groups of cells to initiate reentry in tissue.
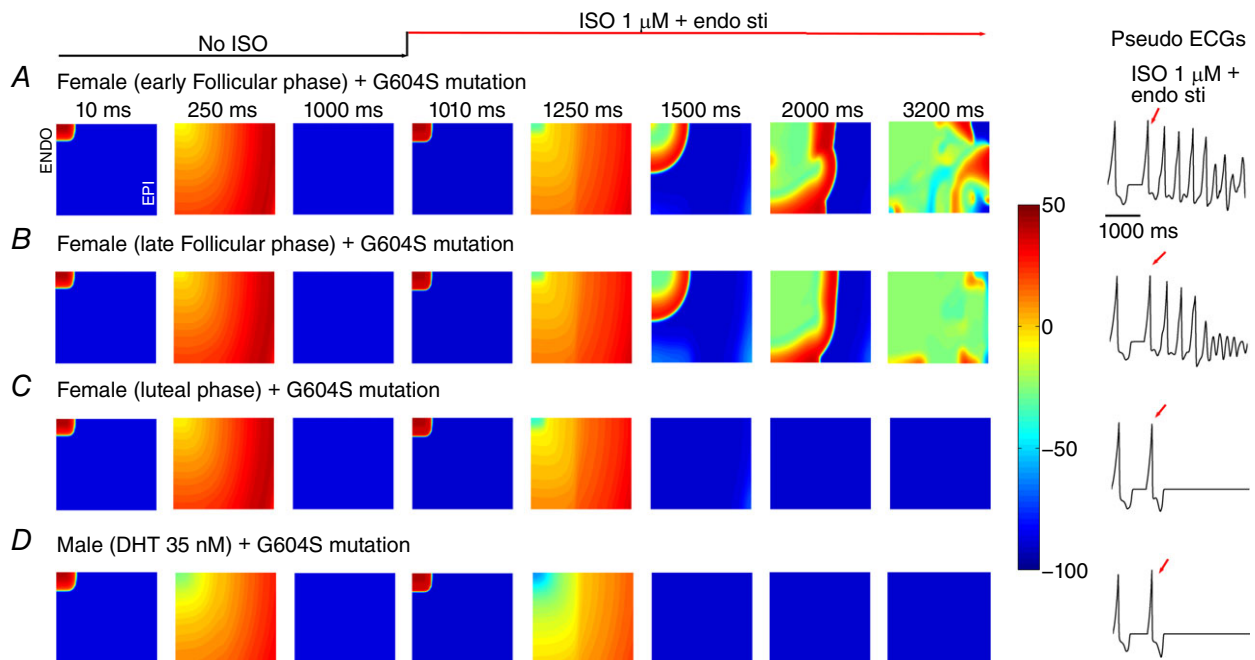

Figure 7. Female sex is predicted to increase susceptibility to reentrant arrhythmia following acute SNS stimulation in the setting of inherited LQT2 syndrome
A–C, predicted reentrant wave following SNS on female heterogeneous tissue (5.4 cm × 6.6 cm) containing an endocardial region (tissue columns 1–160) and an epicardial region (tissue columns 161–360) based on recordings from human tissue, and anisotropic conduction in the presence of female hormones during the early follicular (*A*), late follicular (*B*) and luteal (*C*) phases of the menstrual cycle. *D*, no arrhythmia was predicted in male tissue with 35 nM testosterone. Computed electrograms from simulated tissues are shown in the right panels.

Structure-based mechanisms of arrhythmia vulnerability in females

Similar to female predominance of arrhythmia in the acquired setting, which suggests interactions between hERG, dofetilide and oestradiol, the female predominance of inherited arrhythmia linked the the G604S mutations, suggests that oestradiol may differentially interact with the mutant hERG channel compared to WT. To probe a possible molecular mechanism, we utilized the molecular docking of oestrogen throughout hERG and identified a second E2 binding site located near the pore loop region discovered in molecular docking studies performed with hERG Model 1 (based on the Eag1 template) described above that involves a number of residues implicated in gating dynamics. In the WT, this site is exposed to the lipid bilayer, allowing for easy access to oestradiol (Fig. 10*A*, left). The estimated binding affinity of -5.4 kcal mol^{-1} places E2 in the cohort of weak binders with the estimated pIC$_{50}$ (a negative log of 50% inhibition coefficient) <4.5, comparable to carvedilol block of WT hERG (Durdagi *et al.* 2012; Anwar-Mohamed *et al.* 2014). The MD simulations of E2 to this binding site show that oestradiol displays a very broad range of docking poses, and can rapidly unbind and diffuse away from this low-affinity site to lipid bilayer. Notably, this site hosts the G604S pore loop mutation, implicated in female proclivity to arousal arrhythmia.

This pore loop region appears to be a unique structural feature of both Eag and Erg channels. MD simulations

suggest that E2 dissociates rapidly from this site in WT and hence is unlikely to impair function of WT hERG channel. In order to investigate how this specific mutation G604S affects oestradiol binding at the pore loop receptor site, we mutated our WT hERG model accordingly, and again used molecular docking to identify key binding motifs, shown in the left and right panels of Fig. 10*A* for WT and G604S, respectively.

The MD simulations of the G604S–E2 complex are in stark contrast with results we obtained for WT channel. Molecular docking alone results in indistinguishable binding enthalpies of E2 between WT and G604S: -6.1 kcal mol^{-1} *vs*. -5.4 kcal mol^{-1}, respectively. However, MD simulations reveal major differences in conformational dynamics of the pore loop region with E2 bound in WT and G604S. The clustering of E2 poses on the hERG extracellular loop in WT and mutant proteins is shown in Fig. 10*B*. The RMS fluctuations show that the mobility/flexibility is much lower when E2 is bound to the G604S mutant compared to WT (Fig. 10*C* and Appendix Fig. A5). When E2 is bound to the G604S mutant, interaction remains stable throughout the 50 ns MD, whereas E2 departs from the WT channel within 20 ns (Fig. 10*C*).

These results suggest that the pore loop mutation enhances binding of E2 to the hERG channel. They also suggest that the enhanced affinity is not due to key interactions between the G604 mutated residue and E2, but rather the interplay between conformational and flexibility changes resulting from the mutation. Vandenberg and
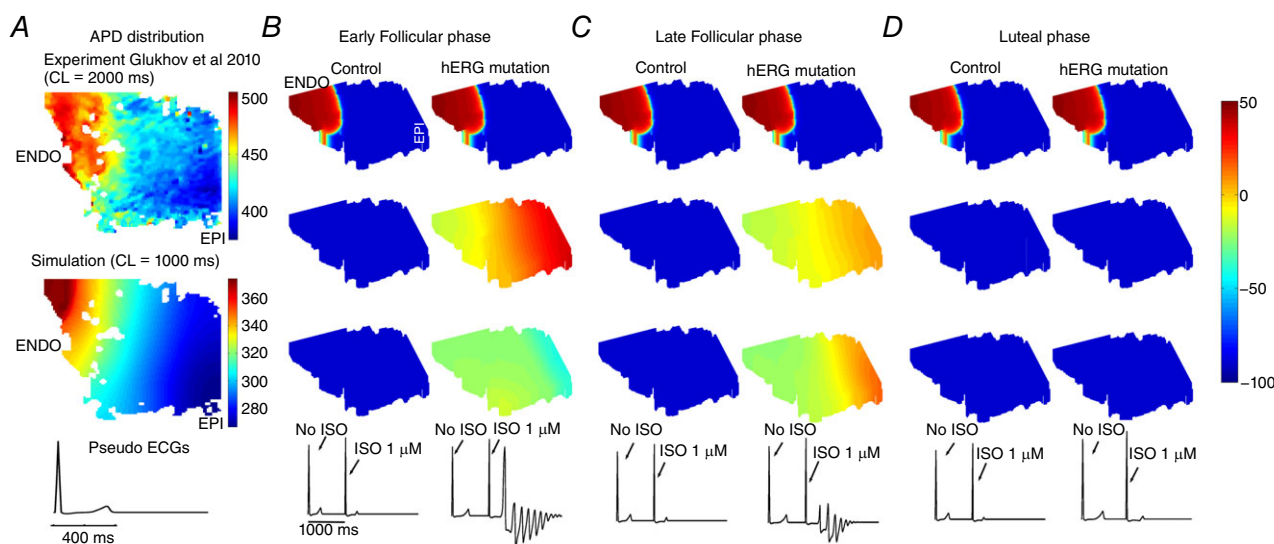

Figure 8. *In silico* **3D reconstructed human long-QT syndrome type 2 female LV wedge based on Glukhov *et al.* (2010) paced with SNS applied**

A, reconstruction of a human tissue *in silico* from normal female explanted heart at a pacing rate of 1 Hz. Experimental data from normal human left ventricle (Glukhov *et al.* 2010) shown at the top. *B–C*, simulated tissue and pseudo ECG are shown in the bottom panel. In the early follicular (*B*) and late follicular (*C*) phases of the menstrual cycle, SNS application initiates arrhythmia. *D*, the luteal phase is not predicted to be sensitive to SNS. APD variability is indicated by the colour scale from long APD$_{80}$ (red) to short (blue).

colleagues (Pages *et al.* 2009) suggested that dynamics and flexibility of this region is critical for the stability of the selectivity filter and therefore is expected to play a substantial role in inactivation dynamics.

Discussion

'It has only been possible to collect a few figures for normal women, but so many of these fall outside the range for normal men,' wrote Bazett in his 1920 analysis of cardiac electrical activity (Bazett, 1997). Nearly a century has passed since the initial recognition of sex-based differences in cardiac electrical activity. Yet, even now, there is a little known about the *structural and functional mechanisms* underlying the sex-based differences that predispose human women to inherited and acquired long-QT syndrome and associated torsade de pointes (TdP) arrhythmias (Makkar *et al.* 1993; Locati *et al.* 1998; Salama & Bett, 2014).

Recent experimental studies in a rabbit model of acquired long-QT syndrome show an increased risk for arrhythmia and TdP in adult female hearts that is not observed in pre-pubescent female or adult male

hearts (Liu *et al.* 2005; Sims *et al.* 2008). In these studies, oestrogen-dependent genomic upregulation of $I_{Ca,L}$ and I_{NCX} were implicated as possible contributors to TdP in females (Chen *et al.* 2011; Yang *et al.* 2012). However, these studies did not address the impact of the autonomic nervous system that apparently impacts arrhythmia risk in females. Our predictions (Fig. 9) do support the idea that upregulation of NCX may promote arrhythmias in females. A population study by Kim *et al.* (2010) showed that 82% of observed arousal-induced arrhythmias occurred in females.

Because sympathetic discharge is a well-recognized factor in triggering TdP in long-QT syndrome patients, the combined effects of protein kinase A (PKA) phosphorylation and sex hormones on ion channels have recently been studied experimentally (Furukawa & Kurokawa, 2007; Nakamura *et al.* 2007; Vaseghi & Shivkumar, 2008). Progesterone was shown to prevent PKA-mediated increases in depolarizing current through the $I_{Ca,L}$, while enhancing the effect of PKA-induced repolarizing I_{Ks} (Nakamura *et al.* 2007). The net effect of these two changes is to increase repolarizing current and reduce APD. In this study, we also included new
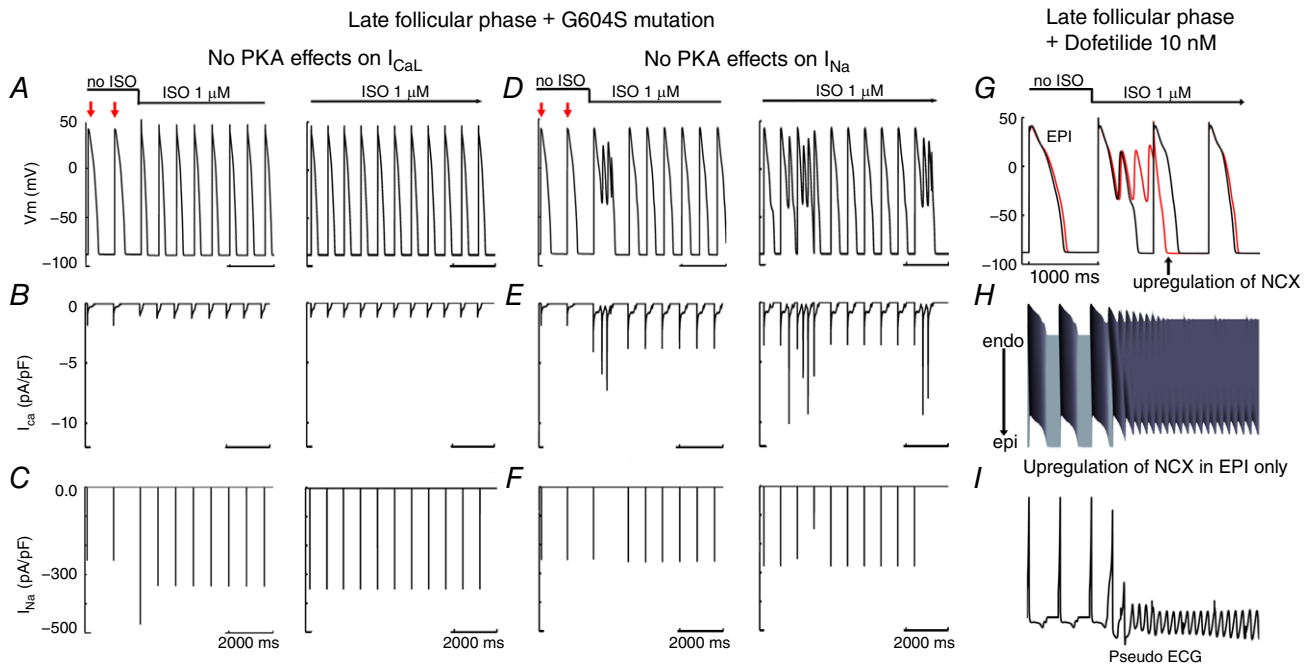

Figure 9. Ionic mechanisms of simulated arousal via sympathetic stimulation in the setting of inherited or acquired LQT during late follicular phase
Since ISO increased I_{caL} and I_{Na}, here we investigated which current induced EAD. *A–C* suggested that when we removed PKA effects on I_{caL} (*B*), there was no EAD induction. The 399th–400th (red arrows) are shown prior to application of SNS. Upon SNS application, the pacing cycle length was increased to 800 ms for 100 beats. The last 11 beats (BCL = 800 ms, under SNS stimulations) are shown in the right panels. *D–F* show that eliminating PKA effects on I_{Na} (*F*) does not suppress EAD-triggered activity. *G*, I_{NCX} densities were increased by 2-fold (Chen *et al.* 2011) in epi cell (red line) compared with no changes in I_{NCX} (black line). *H*, transmural 1-dimensional tissue models with upregulation of NCX in epicardium. *I*, the pseudo ECG is shown beneath the tissue simulation.
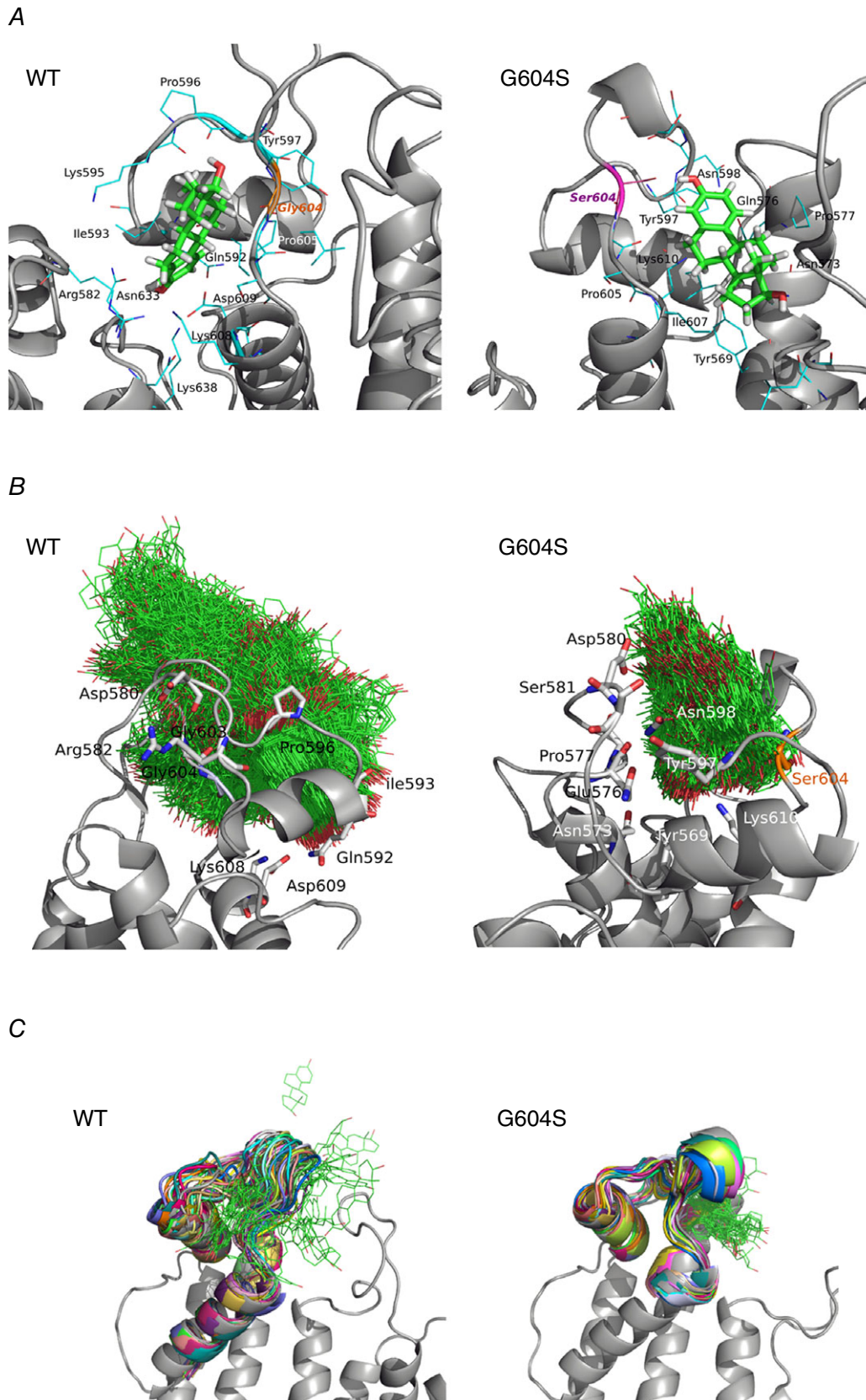
Figure 10. Oestradiol (E2) binding to a pore loop site of hERG from molecular docking (*A*), and molecular dynamics (*B* and *C*) simulations for wild-type (WT; left) and G604S mutant hERG channel (right)

A, top scoring docking poses for dofetilide in the pore loop site shown together with coordinating residues within 3.5 Å for mapped binding sites. *B*, E2 positions (shown in green wireframe representation) are mapped from the frames collected in 40 ns MD for WT and G604S in order to illustrate the conformational space explored by the ligand in the two systems. It is apparent that E2 is kinetically stabilized (trapped) in the G604S mutant, while it is unable to bind stably in WT and leaves the binding pocket within 20 ns of MD simulation. *C*, a G604S mutation is predicted to enhance stability of the bound E2 (green wireframe) in the binding pocket by controlling binding site flexibility: the mutation stabilizes the binding site allowing for E2 to remain in the pocket. In contrast, E2 readily leaves binding pocket in the WT hERG protein and diffuses away to the lipid bilayer. Shown are 32 selected frames from the first 15 ns of molecular dynamics simulation for E2/WT and E2/G604S are shown in different colours.

data showing the effects of testosterone on the L-type Ca^{2+} current in the presence of isoproterenol (Fig. 1). Just as has been shown for progesterone in a previous study (Nakamura *et al.* 2007), testosterone application blunted the isoproterenol-induced enhancement of the L-type Ca^{2+} current. This provides a plausible mechanism for testosterone protection against arousal-induced arrhythmias: a reduction in L-type Ca^{2+} current allows for greater rate-dependent shortening of the male action potential and reduces arrhythmia likelihood.

Women are disproportionately affected by inherited forms of long-QT syndrome associated with hERG pore loop mutations as well as by acquired long-QT syndrome, which results from unintended off-target block of the major cardiac repolarizing current I_{Kr}, encoded by the hERG gene and characterized by prolongation of the QT interval. The basis of our study was the hypothesis that oestrogen will acutely increase arrhythmia vulnerability and that progesterone will protect against arrhythmia initiation, especially in the setting of sympathetic stimulation, a major factor in triggering TdP. This hypothesis is based on published data showing that oestrogen interacts directly with the promiscuous hERG channel, reduces repolarizing I_{Kr} current and increases the rate of channel deactivation (Kurokawa *et al.* 2008). Kurokawa and co-authors proposed that aromatic centroid of E2 may be responsible for increasing the sensitivity of hERG block by E4031 via interaction with the aromatic side chain of Phe-656 and aromatic rings of the hERG blocker.

Kurokawa and co-authors have also shown that in the presence of E2, hERG is markedly more sensitive to block by drugs and that the concentration of E2 fluctuates throughout the menstrual cycle, from the peak follicular phase serum E2 level of 1 nM to 0.7 nM in the luteal phase (Kurokawa *et al.* 2008). Since E2 has dramatic effects on sensitivity to hERG block within this range, it stands to reason that susceptibility to drug-induced arrhythmia by hERG block may also vary through the menstrual cycle, but the exact mechanism of potential concomitant effects on common blocker action remain unknown. The predictions from molecular modelling studies based on bacterial KcsA and MthK (Perry *et al.* 2004; Stansfeld *et al.* 2007) channels or the mammalian channel Kv1.2 (Durdagi *et al.* 2010; Stary *et al.* 2010) concur with the experimental

findings that have revealed two key residues responsible for drug stabilization in the hERG1 cavity, e.g. Y652 and F656 (Lees-Miller *et al.* 2000; Mitcheson *et al.* 2000; Ficker *et al.* 2001; Vandenberg *et al.* 2001; Fernandez *et al.* 2004; Durdagi *et al.* 2012). Model studies reproduced this feature in studies of hERG blockers such as dofetilide, KN-93 and other common high-affinity blockers (Durdagi *et al.* 2011, 2012).

Previous studies of high- and low-affinity blockers such as dofetilide, astemizole and haloperidole suggest that an 'ideal' high-affinity blocker should simultaneously interact with F656, Y652 and/or A653 at the inner cavity of hERG, and form hydrogen bonds with T623 and S624 from the pore helix (Mitcheson *et al.* 2000; Lees-Miller *et al.* 2000; Ficker *et al.* 2001; Fernandez *et al.* 2004; Durdagi *et al.* 2011, 2012; Vandenberg *et al.* 2001). The binding data collected from our MD simulations shown in Fig. 4 endorse the presence of these sites accommodating favourable and synergistic binding of both E2 and dofetilide. The distribution of binding energies and binding pockets for E2 and dofetilide suggest a plausible scenario of hormone modification of common blocker action. In the intracellular cavity (IC) of hERG, the presence of E2 only modestly enhances the binding affinity of dofetilide; however, there is less variance in the distribution of binding energies for dofetilide with E2 bound. That is, bound hormone stabilizes the high-affinity site for dofetilide and virtually eliminates binding to a low-affinity site.

The hERG channel exhibits a high degree of homology with the Eag1 channel, the structure of which has recently been determined (Whicher & MacKinnon, 2016). The availability of the Eag1 structure provided us with a new and unique structural template for understanding arrhythmia-associated mutations.

A key feature revealed by the structure is the extended 'extracellular turret'. Indeed, this region is home to the G406S mutation studied here, and we found that it appears to provide a pocket for oestrogen binding that is stabilized by the mutation. The new structural data allowed the revelation of interactions between physiologically important and tightly controlled lipophilic substances such as E2 and functionally important lipid-facing regions of the hERG channel. It is also predicted in our study that E2 binding may impact the channel through

two distinct mechanisms. The first mechanism involves a high-affinity binding site that is located near the pore loop region, which is involved channel kinetics and plays an important role in normal physiology. Post-adolescent females show more than nine times the number of arousal-triggered arrhythmias than men of the same age group, and arousal-triggered events are more than twice as high among female patients exhibiting mutations in the pore loop region of hERG, but not mutations in other regions (Kim *et al.* 2010). We hypothesized that pore loop mutations may modify the oestrogen interaction with hERG. Indeed, this notion is corroborated by our findings, which suggest that E2 binds with higher affinity in the hERG model with the pore loop G604S mutation.

The second mechanism involves another high-affinity binding site for E2, located in the intracellular cavity of hERG in the vicinity of Y652, a residue crucial for the channel block. This suggests that E2 may enhance the action of common blockers, such as dofetilide, as predicted by our binding enthalpy calculations. It is also probable that the mechanisms co-exist, depending on the physiologically driven concentration fluctuations of E2 in cell membranes. Establishing a connection between these two mechanisms of action is a goal for our future studies.

The present study focuses on the role that changes in sympathetic tone play in triggering arousal-induced arrhythmia. It should be noted that there are also sex-related differences in parasympathetic tone that we have not considered in this study. It has been demonstrated that parasympathetic influence on cardiac function is greater in females than males (Dart *et al.* 2002). Elevated parasympathetic tone, which is associated with greater heart rate variability, was found to be greater in premenopausal women and postmenopausal women receiving hormone replacement therapy, suggesting that oestrogen may be responsible (Liu *et al.* 2003). Because of this, it is conceivable that abrupt termination of parasympathetic input also contributes to arousal-induced arrhythmias, since vagal withdrawal has been shown to result in an increase in cAMP production that potentiates sympathetic responses (Belevych *et al.* 2001; Harvey & Belevych, 2003).

Limitations of the current study

There are several limitations in our study. While the O'Hara–Rudy model was extensively validated in reproducing experimentally observed rate dependence in single cells, the model overestimates the rate dependence of APD in human tissue compared to experiments reported by Franz *et al.* (1988). We also did not consider the presence of other prevalent disease states such as diabetes that have a sex difference component (Shimoni *et al.* 2009).

An important limitation in the interpretation of structural modes of E2 binding to hERG is an absence of a high-resolution experimental structure of the channel. In this study, we resorted to using homology models in our simulations, which depend on the availability of high-resolution experimental template structures, in the desired conformational state, and with high sequence identity. We therefore chose suitable templates (Eag1 and Kv1.2) for our models that allowed us to study two distinct regions of interest in hERG: the pore loop region and the intracellular cavity. While we recognize the inherent limitations of using homology models, there is, importantly, remarkable consensus for crucial drug binding sites in both models that we used.

We also acknowledge that our molecular simulation approach returns only binding enthalpy distributions, which, in the absence of the entropic and diffusion data that are crucial for quantitative drug–channel thermodynamic and kinetic predictions, are not able to unambiguously predict quantitative indices of current inhibition. We are planning further studies now with mapping free energy and diffusion profiles to compute 'on' and 'off' channel-hormone interaction rates for the kinetic models to evaluate impact of hormone binding on the channel current blockade. Our current study reveals the first mechanistic models of how E2 could potentially enhance hERG blockade. However, dofetilide is known to exhibit several modes of binding to hERG and our first simulation here suggests that oestradiol helps to stabilize one of them in the open pore of the hERG channel. Furthermore, based on work of Sanguinetti (Chen *et al.* 2002) and studies that followed (Rodriguez-Menchaca *et al.* 2006; Stork *et al.* 2007; Lees-Miller *et al.* 2015), we may expect a state-dependent blockade by dofetilide and thus will need to evaluate binding of a hormone to different states. Whether these are separate mechanisms or ones that can coexist are the questions we intend to study in the near future. This work will refine different E2 binding modes, their affinities and kinetics through a combination of experimental and computational studies.

The computational modelling and simulation approach has allowed us to explore the complex non-linear interplay between processes that underlie differences in risk to acquired long-QT-dependent arrhythmias. They also allow us to predict the 'perfect storm' of hormone concentration, I_{Kr} derangement and sympathetic stimulation that may explain one mechanism of increased proclivity to arousal arrhythmia in females. The results of this study suggest specific therapeutic anti-arrhythmic strategies for women with long-QT syndrome, which may include specific hormone replacement therapy, as well as suggested and counter-indicated drugs. To realize the most basic biological mechanisms underlying sex-based differences in long-QT syndrome risk and susceptibility to TdP arrhythmias is the critical first step to set the stage for specific sex-based diagnosis and therapeutic targeting of cardiac disease.

Appendix: Simulation of genomic sex steroid hormone effects

Female hearts had reduced expression of the K(C)-channel subunits HERG, minK, Kir2.3, Kv1.4, KChIP2, SUR2, and Kir6.2, and lower mRNA expression of connexin43 and phospho-lamban compared to males. Experiments demonstrated concurrence of changes between gene and protein expression for HERG, minK, Kv1.4, KChIP2, IRX5, Nav1.5 and connexin43 (Nav1.5-expression showed no male–female differences) (Gaborit *et al.* 2010). Details are given in Table A1.

Table A1. Sex-based differences in ion channel subunit expression from non-diseased ventricles used in the computational model

Channels in the model	Gene	Epi		Endo	
		Male	Female	Male	Female
I_{Ks}	KvLQT1	104.2	77.5	90.4	109.6
	MinK(KCNE1)	13.6 ± 1.4	7.3 ± 5	11.9 ± 4.2	5.8 ± 2.6
		m*↑	f*↓	m**↑	f**↓
	Ratio	1.04 ± 0.04	0.87 ± 0.14	1 ± 0.12	0.83 ± 0.07
	Functions	Co-expression of KvLQT1 and MinK shifts the voltage to more positive voltages. Also it increases amplitude of expressed current. Only MinK shows significant differences between male and female. The stoichiometry of KCNE1:KCNQ1 in I_{Ks} channels is a fixed 2:4 (Nakajo *et al.* 2010). The ratio was calculated by modified the 1/3 of current activity depending on MinK.			
I_{Kr}	hERG(Kv11.1)	179.5 ± 6.4	144.2 ± 41.1	164.8 ± 54.9	130.5 ± 65
		m*↑	f*↓	↑	↓
	Ratio	1.09 ± 0.039	0.875 ± 0.25	1 ± 0.33	0.79 ± 0.39
I_{K1}	Kir2.1	94.5	93.8	104.1	79.7
	Kir2.2	111.1	115.3	93.6	104.5
	Kir2.3	91.2 ± 31.8	21.4 ± 10.6	92.7 ± 26.8	55.2 ± 21.5
		m*↑	f*↓	m**↑	f**↓
	Ratio	0.98 ± 0.12	0.74 ± 0.04	1 ± 0.09	0.86 ± 0.077
	Functions	Kir2.x channels mediate cardiac I_{K1} (Dhamoon *et al.* 2004); however, only Kir2.3 is significantly different. The ratio was calculated by changing the 1/3 of Kir2.3 channel activity.			
$I_{to,s}$	Kv1.4	12.1 ± 3.3	5.4 ± 3.8	20.2 ± 4.0	12.9 ± 5.2
		m*↑	f*↓	m**↑	f**↓
	Ratio	0.6 ± 0.16	0.26 ± 0.19	1 ± 0.2	0.64 ± 0.26
I_{NaK}	ATPasea1	207.7 ± 67	513.4 ± 134.6	269.0 ± 70.3	622.5 ± 287.7
		m*↓	f*↑	m**↓	f**↑
	a3	1481 ± 267	917.8 ± 416.7	1547.6 ± 299.5	1014.2 ± 294.5
		m*↑	f*↓	m**↑	f**↓
	Ratio	0.94 ± 0.18	0.7 ± 0.3	1.0 ± 0.2	0.79 ± 0.26
	Functions	a3 is about 2-fold more active than a1 in LV (Gaborit *et al.* 2007). The ratio was calculated depending on 1/3 of a1 and 2/3 of a3.			
I_{pCa}	PMCA1	31.7	46.4	44.1	48.1
	PMCA4	377.0 ± 57.2	682.1 ± 265.9	426.8 ± 116.6	685.2 ± 379.7
		m*↓	f*↑	m↓	f↑
	Ratio	0.88 ± 0.13	1.6 ± 0.6	$1.\pm 0.27$	1.6 ± 0.89
	Functions	PMCA1 serves a critical housekeeping function that is required for the maintenance of basic cellular function (Brini, 2009). PMCA4 nearly ubiquitous distribution has a similar role to that of PMCA1. PMCA4 was reported much more activity than PMCA1 in LV (Gaborit *et al.* 2007), and there are no differences between sexes in PMCA1. The ratio was calculated depended only on the PMCA4.			
I_{up}	SERCA2	4850.5 ± 146	6728.4 ± 1876.1	3410.4 ± 982.1	3921.9 ± 1760.7
		m*↓	f*↑	m	f
	Ratio	1.42 ± 0.04	1.97 ± 0.55	1 ± 0.28	1.15 ± 0.5
Calmodulin	CALM1	1329.5	991.9	879.8	1122.7
	CALM3	1326.9 ± 220	1955.5 ± 372.2	1206.9 ± 187.7	1600.5 ± 242.9
		m*↓	f*↑	m**↓	f**↑
	Ratio	1.07 ± 0.12	1.41 ± 0.2	1 ± 0.1	1.21 ± 0.14
	Functions	CALM3 is more activity than CALM1 (~2-fold in LV) (Gaborit *et al.* 2007). The ratio was obtained by changing the 2/3 of activity depends on CALM3.			

(Continued)

Table A1. Continued

Channels in the model	Gene	Epi		Endo	
		Male	Female	Male	Female
Gap-junction	Cx43	1124.1 ± 357	728.6 ± 274.1	1196.3 ± 311.7	810.9 ± 333.9
		m* ↑	f* ↓	m** ↑	f** ↓
	Ratio	0.94 ± 0.3	0.61 ± 0.24	1.0 ± 0.26	0.68 ± 0.28

Ratios are relative to the male endocardial cell as we published previously (Yang & Clancy, 2012). *Differences between male and female in Epi is statistically significant. **Differences between male and female in Endo are statistically significant.

Table A2. Simulated effects of progesterone on I_{Ks} and $I_{Ca,L}$

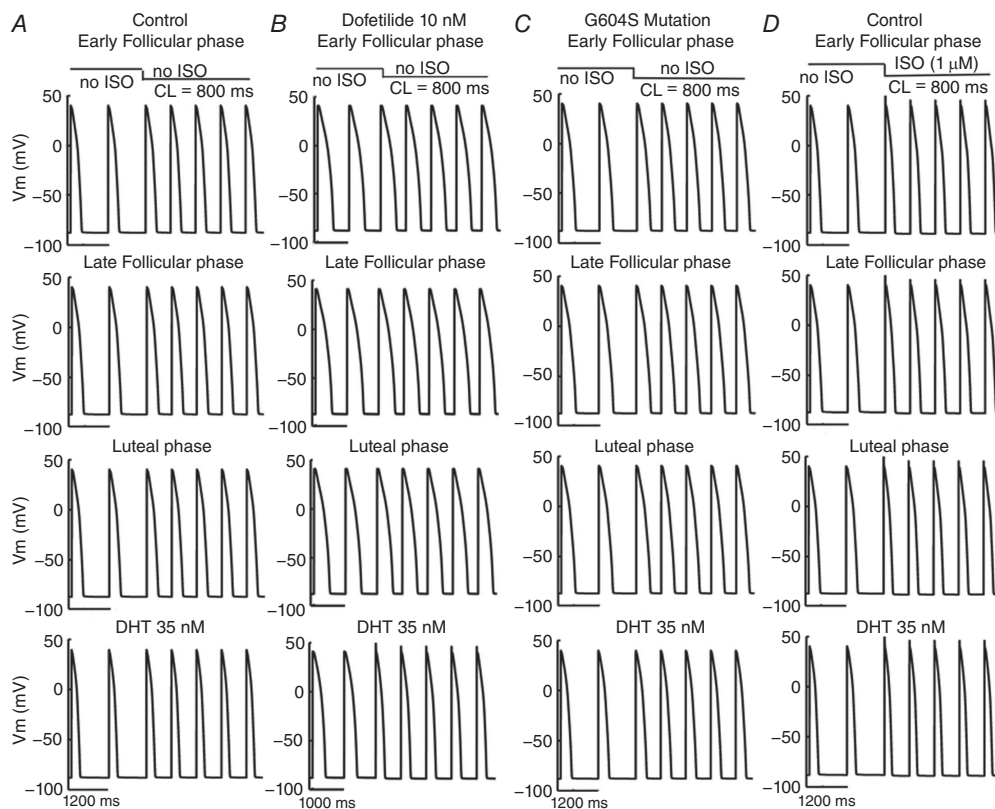| Channel	Progesterone (baseline)		Progesterone (SNS stimulations)	
	2.5 nM	40.6 nM	2.5 nM	40.6 nM
I_{Ks}	1.19	1.4	3.488	3.52
I_{CaL}	1.0	1.0	2.5	2.5
Kinetics of I_{CaL}	No effects		$d_{ss} = 1.0/\{1.0 + \exp[(-(v + 3.94 + 16 - 1.5))/4.73]\}$ $f_{ss} = 1.0/\{1.0 + \exp[(v + 19.58 + 8.0 + 1.7)/3.596]\}$	$d_{ss} = 1.0/\{1.0 + \exp[(-(v + 3.94 + 16 - 4.4))/5.23]\}$ $f_{ss} = 1.0/\{1.0 + \exp[(v + 19.58 + 8.0 + 3.7)/3.096]\}$
Reference	Nakamura *et al.* (2007)			

Figure A1. Single cell action potentials during simulated arousal via sympathetic stimulation in the setting of control or the G604S mutation
Action potentials are shown following pacing for 400 paced beats at a cycle length of 1000 ms in single simulated endocardial cells. The 399th and 400th paced beats are shown, after the pacing frequency was increased to 800 ms with or without SNS applied. A, control case with no SNS applications. B, dofetilide with no SNS applications. C, G604S mutation with no SNS applications. D, control case with SNS applied after 400 beats.

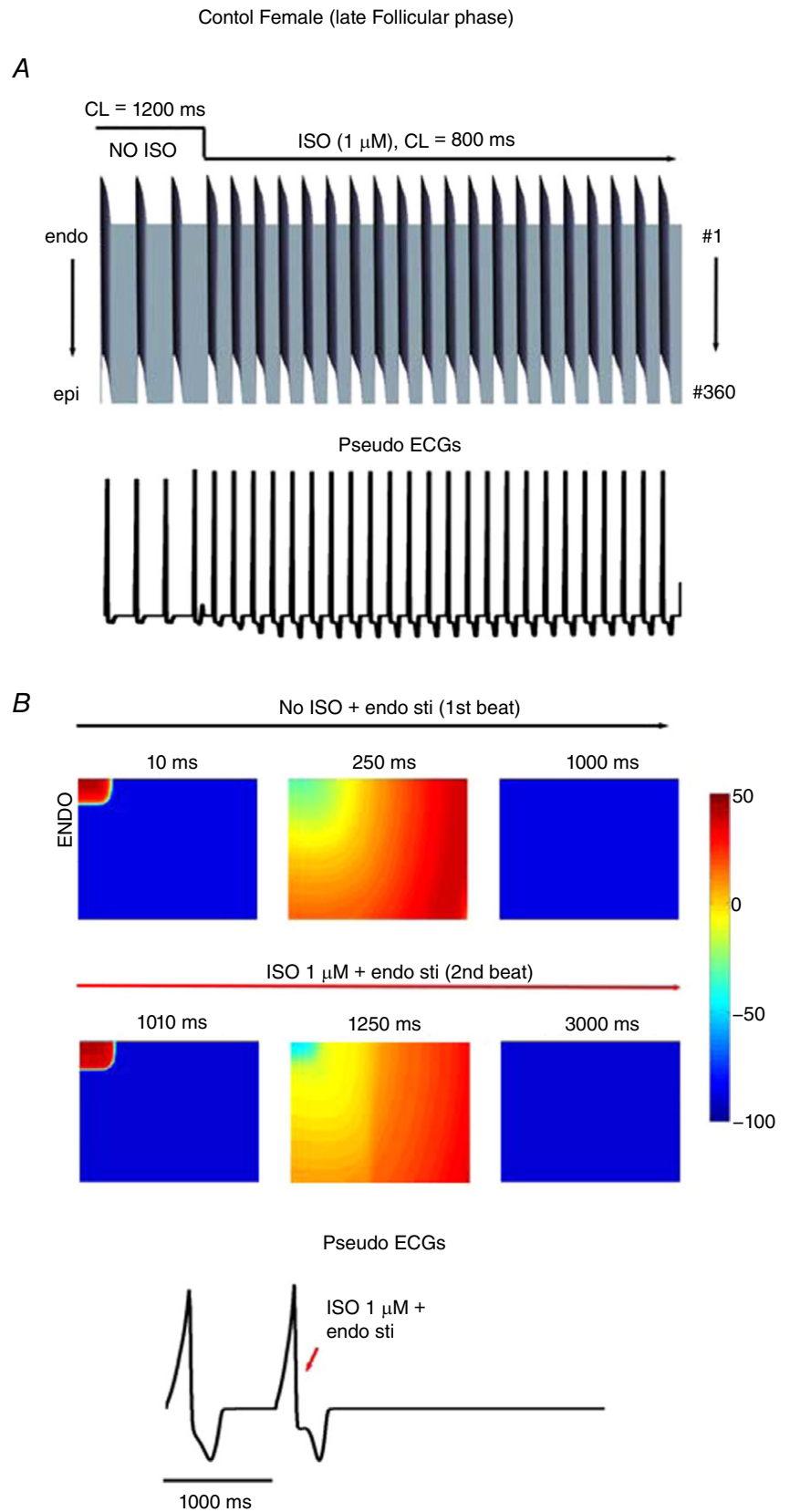Contol Female (late Follicular phase)

Figure A2. Human cardiac electrophysiology predicted in female late follicular phase (no mutation) transmural tissue models and simulated pseudo-ECGs during SNS

A, simulated 1-dimensional action potentials (APs) are shown following pacing for 400 beats at 1200 ms pacing frequency. The 398th–400th paced beats are shown prior to application of SNS. Upon SNS application, the pacing frequency was increased to 800 ms. The pseudo ECG is shown beneath the tissue simulation. Time is shown on the *x*-axis and voltage on the *z*-axis. *B*, simulated combined effects of oestradiol and progesterone on female (no mutation) 2-dimensional tissues during the late follicular phase of the menstrual cycle.
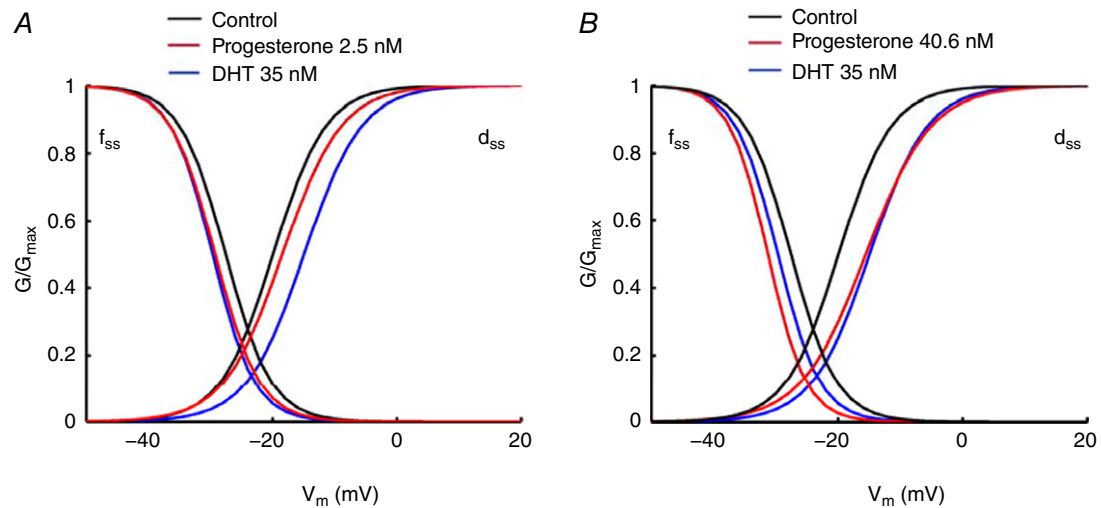
Figure A3. The L-type Ca²⁺ window current

Steady-state activation (d_{ss}) and steady-state inactivation (f_{ss}) show the I_{CaL} window current during SNS via ISO. *A*, DHT 35 nM (blue lines) indicated a smaller window current compared to progesterone 2.5 nM (red lines). *B*, high concentration of progesterone (40.6 nM, red lines) reduced the I_{CaL} window current.
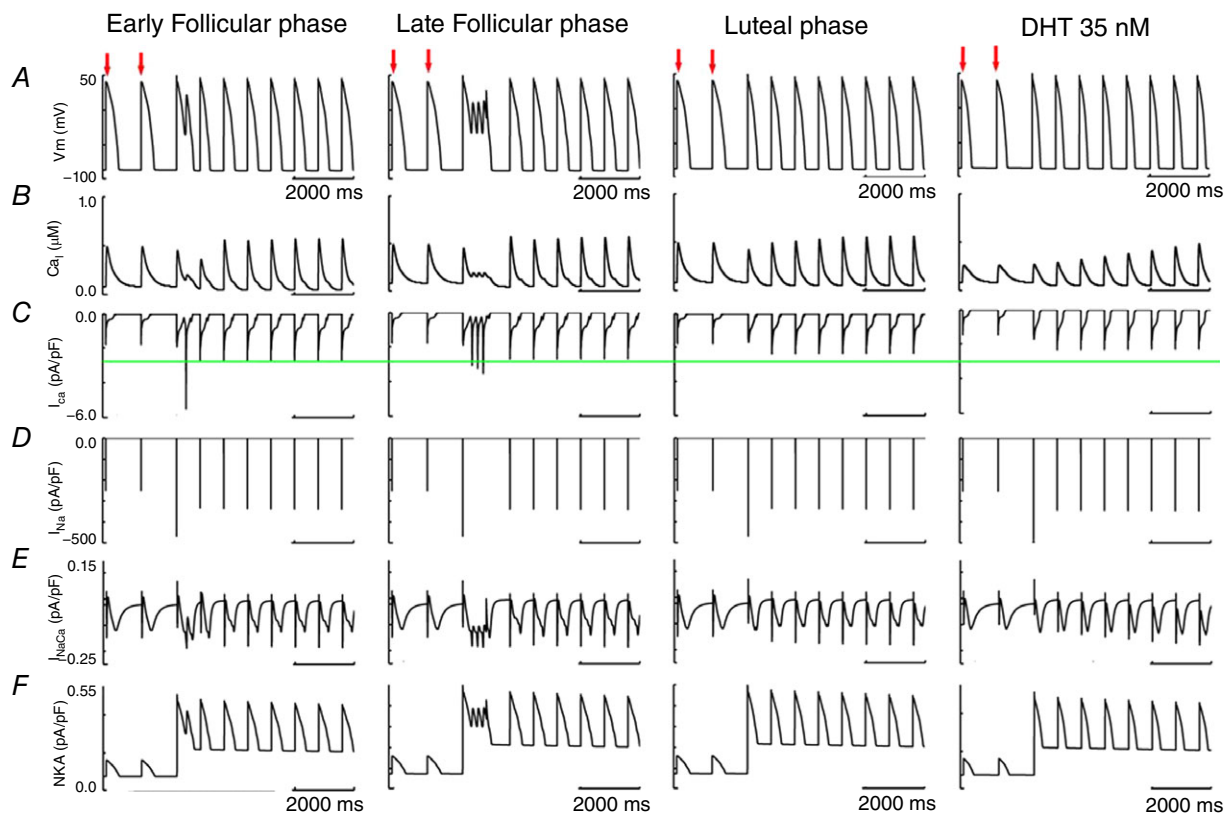

Figure A4. Ionic mechanisms of simulated arousal via sympathetic stimulation in the setting of the G604S mutation causing inherited LQT2 syndrome

A, cellular APs. *B*, intracellular Ca²⁺ concentration. *C*, L-type Ca²⁺ current. *D*, Na⁺ current. *E*, Na⁺/Ca²⁺ exchange current. *F*, Na⁺/K⁺-ATPase (NKA). Same pacing protocol was used as in Fig. 2. The 399th–400th paced beats (red arrows) are shown prior to application of SNS. Upon SNS application, the pacing frequency was increased to 800 ms for 100 beats. *C* shows the peak of I_{CaL} was lower in luteal phase or with DHT 35 nM.
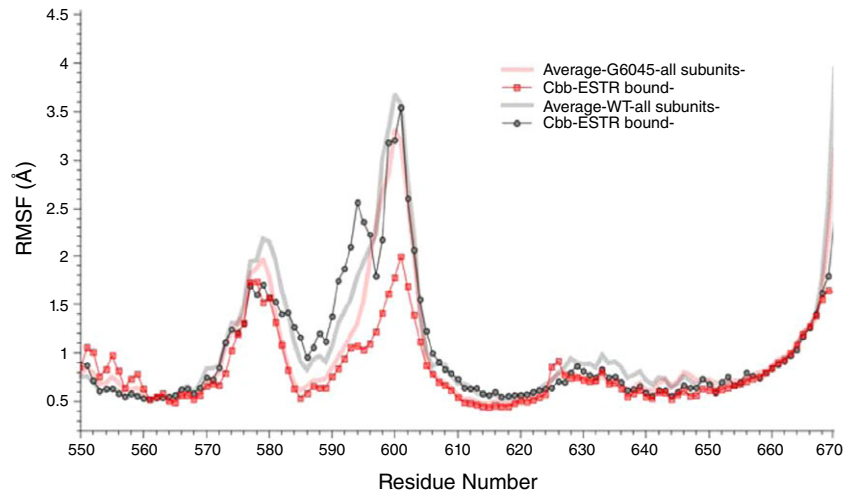
Figure A5. RMS fluctuations per residue (550–670) for all the subunits of WT (thick grey line) and G604S (thick red line), E2 bound to WT chain C (black circles) and E2 bound to G604S chain C (red squares)
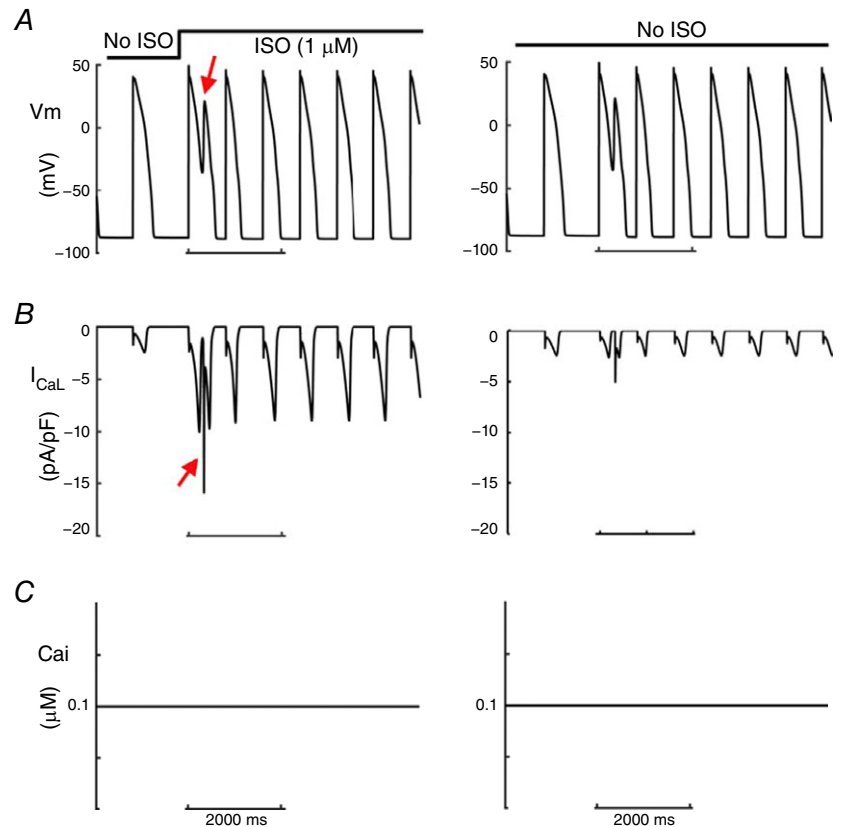

Figure A6. Action potential voltage clamp of simulated arousal via sympathetic stimulation in the setting of the G604S mutation causing inherited LQT2 Syndrome
A, cellular action potentials were clamped to the voltages shown in Fig. A4. B, L-type Ca^{2+} current. C, intracellular Ca^{2+} concentration was clamped to the diastolic rest concentration. Same pacing protocol was used as in Fig. A4. When Ca^{2+}-dependent inactivation is reduced (Ca^{2+} concentration clamped to diastolic level), with an EAD voltage clamp protocol, the Ca^{2+} current is even larger, suggesting a strong effect of ISO that is usually tempered by Ca^{2+}-dependent inactivation. In the absence of ISO, the effect is much smaller (right panels).

References

Anneken L, Baumann S, Vigneault P, Biliczki P, Friedrich C, Xiao L, Girmatsion Z, Takac I, Brandes RP, Kissler S, Wiegratz I, Zumhagen S, Stallmeyer B, Hohnloser SH, Klingenheben T, Schulze-Bahr E, Nattel S & Ehrlich JR (2016). Estradiol regulates human QT-interval: acceleration of cardiac repolarization by enhanced KCNH2 membrane trafficking. *Eur Heart J* **37**, 640–650.

Anwar-Mohamed A, Barakat KH, Bhat R, Noskov SY, Tyrrell DL, Tuszynski JA & Houghton M (2014). A human ether-á-go-go-related (hERG) ion channel atomistic model generated by long supercomputer molecular dynamics simulations and its use in predicting drug cardiotoxicity. *Toxicol Lett* **230**, 382–392.

Bai CX, Kurokawa J, Tamagawa M, Nakaya H & Furukawa T (2005). Nontranscriptional regulation of cardiac repolarization currents by testosterone. *Circulation* **112**, 1701–1710.

Bazett HC (1997). An analysis of the time-relations of electrocardiograms. *Ann Noninvasive Electrocardiol* **2**, 177–194.

Belevych AE, Sims C & Harvey RD (2001). ACh-induced rebound stimulation of L-type Ca^{2+} current in guinea-pig ventricular myocytes, mediated by $G\beta\gamma$-dependent activation of adenylyl cyclase. *J Physiol* **536**, 677–692.

Benkert P, Biasini M & Schwede T (2011). Toward the estimation of the absolute quality of individual protein structure models. *Bioinformatics* **27**, 343–350.

Best RB, Zhu X, Shim J, Lopes PE, Mittal J, Feig M & Mackerell AD Jr (2012). Optimization of the additive CHARMM all-atom protein force field targeting improved sampling of the backbone ϕ, ψ and side-chain χ_1 and χ_2 dihedral angles. *J Chem Theory Comput* **8**, 3257–3273.

Bidoggia H, Maciel JP, Capalozza N, Mosca S, Blaksley EJ, Valverde E, Bertran G, Arini P, Biagetti MO & Quinteiro RA (2000). Sex differences on the electrocardiographic pattern of cardiac repolarization: possible role of testosterone. *Am Heart J* **140**, 678–683.

Brini M (2009). Plasma membrane Ca^{2+}-ATPase: from a housekeeping function to a versatile signalling role. *Pflugers Archiv* **457**, 657–664.

Burke JH, Ehlert FA, Kruse JT, Parker MA, Goldberger JJ & Kadish AH (1997). Gender-specific differences in the QT interval and the effect of autonomic tone and menstrual cycle in healthy adults. *Am J Cardiol* **79**, 178–181.

Chen G, Yang X, Alber S, Shusterman V & Salama G (2011). Regional genomic regulation of cardiac sodium-calcium exchanger by oestrogen. *J Physiol* **589**, 1061–1080.

Chen J, Seebohm G & Sanguinetti MC (2002). Position of aromatic residues in the S6 domain, not inactivation, dictates cisapride sensitivity of HERG and eag potassium channels. *Proc Natl Acad Sci USA* **99**, 12461–12466.

Dart AM, Du XJ & Kingwell BA (2002). Gender, sex hormones and autonomic nervous control of the cardiovascular system. *Cardiovasc Res* **53**, 678–687.

Demolis JL, Funck-Brentano C, Ropers J, Ghadanfar M, Nichols DJ & Jaillon P (1996). Influence of dofetilide on QT-interval duration and dispersion at various heart rates during exercise in humans. *Circulation* **94**, 1592–1599.

Dhamoon AS, Pandit SV, Sarmast F, Parisian KR, Guha P, Li Y, Bagwe S, Taffet SM & Anumonwo JM (2004). Unique Kir2.x properties determine regional and species differences in the cardiac inward rectifier K^+ current. *Circ Res* **94**, 1332–1339.

Dighe AS, Moy JM, Hayes FJ & Sluss PM (2005). High-resolution reference ranges for estradiol, luteinizing hormone, and follicle-stimulating hormone in men and women using the AxSYM assay system. *Clin Biochem* **38**, 175–179.

Dorgan JF, Fears TR, McMahon RP, Aronson Friedman L, Patterson BH & Greenhut SF (2002). Measurement of steroid sex hormones in serum: a comparison of radioimmunoassay and mass spectrometry. *Steroids* **67**, 151–158.

Duff HJ, Feng ZP & Sheldon RS (1995). High- and low-affinity sites for [³H]dofetilide binding to guinea pig myocytes. *Circ Res* **77**, 718–725.

Durdagi S, Deshpande S, Duff HJ & Noskov SY (2012). Modeling of open, closed, and open-inactivated states of the hERG1 channel: structural mechanisms of the state-dependent drug binding. *J Chem Inf Model* **52**, 2760–2774.

Durdagi S, Duff HJ & Noskov SY (2011). Combined receptor and ligand-based approach to the universal pharmacophore model development for studies of drug blockade to the hERG1 pore domain. *J Chem Inf Model* **51**, 463–474.

Durdagi S, Subbotina J, Lees-Miller J, Guo J, Duff HJ & Noskov SY (2010). Insights into the molecular mechanism of hERG1 channel activation and blockade by drugs. *Curr Med Chem* **17**, 3514–3532.

Ebert SN, Liu XK & Woosley RL (1998). Female gender as a risk factor for drug-induced cardiac arrhythmias: evaluation of clinical and experimental evidence. *J Womens Health* **7**, 547–557.

Essmann U, Perera L, Berkowitz ML, Darden T, Lee H & Pedersen LG (1995). A smooth particle mesh ewald method. *J Chem Phys* **103**, 8577–8593.

Faber GM & Rudy Y (2000). Action potential and contractility changes in $[Na^+]_i$ overloaded cardiac myocytes: a simulation study. *Biophys J* **78**, 2392–2404.

Fernandez D, Ghanta A, Kauffman GW & Sanguinetti MC (2004). Physicochemical features of the HERG channel drug binding site. *J Biol Chem* **279**, 10120–10127.

Ficker E, Jarolimek W & Brown AM (2001). Molecular determinants of inactivation and dofetilide block in *ether a-go-go* (EAG) channels and EAG-related K^+ channels. *Mol Pharmacol* **60**, 1343–1348.

Franz MR, Swerdlow CD, Liem LB & Schaefer J (1988). Cycle length dependence of human action potential duration in vivo. Effects of single extrastimuli, sudden sustained rate acceleration and deceleration, and different steady-state frequencies. *J Clin Invest* **82**, 972–979.

Furukawa T & Kurokawa J (2007). Regulation of cardiac ion channels via non-genomic action of sex steroid hormones: implication for the gender difference in cardiac arrhythmias. *Pharmacol Ther* **115**, 106–115.

Gaborit N, Le Bouter S, Szuts V, Varro A, Escande D, Nattel S & Demolombe S (2007). Regional and tissue specific transcript signatures of ion channel genes in the non-diseased human heart. *J Physiol* **582**, 675–693.

Gaborit N, Varro A, Le Bouter S, Szuts V, Escande D, Nattel S & Demolombe S (2010). Gender-related differences in ion-channel and transporter subunit expression in non-diseased human hearts. *J Mol Cell Cardiol* **49**, 639–646.

Gabrielsen M, Ravna AW, Kristiansen K & Sylte I (2012). Substrate binding and translocation of the serotonin transporter studied by docking and molecular dynamics simulations. *J Mol Model* **18**, 1073–1085.

Gima K & Rudy Y (2002). Ionic current basis of electrocardiographic waveforms: a model study. *Circ Res* **90**, 889–896.

Glukhov AV, Fedorov VV, Lou Q, Ravikumar VK, Kalish PW, Schuessler RB, Moazami N & Efimov IR (2010). Transmural dispersion of repolarization in failing and nonfailing human ventricle. *Circ Res* **106**, 981–991.

Grundy D (2015). Principles and standards for reporting animal experiments in the journal of physiology and experimental physiology. *J Physiol* **593**, 2547–2549.

Harvey RD & Belevych AE (2003). Muscarinic regulation of cardiac ion channels. *Br J Pharmacol* **139**, 1074–1084.

Hoeker GS, Hood AR, Katra RP, Poelzing S & Pogwizd SM (2014). Sex differences in beta-adrenergic responsiveness of action potentials and intracellular calcium handling in isolated rabbit hearts. *PLoS One* **9**, e111411.

Huang L & Roux B (2013). Automated force field parameterization for nonpolarizable and polarizable models based on ab initio target data. *J Chem Theory Comput* **9**, 3543–3556.

Huikuri HV, Pikkujamsa SM, Airaksinen KE, Ikaheimo MJ, Rantala AO, Kauma H, Lilja M & Kesaniemi YA (1996). Sex-related differences in autonomic modulation of heart rate in middle-aged subjects. *Circulation* **94**, 122–125.

Huo J, Zhang Y, Huang N, Liu P, Huang C, Guo X, Jiang W, Zhou N, Grace A, Huang CL & Ma A (2008). The G604S-hERG mutation alters the biophysical properties and exerts a dominant-negative effect on expression of hERG channels in HEK293 cells. *Pflugers Archiv* **456**, 917–928.

Irwin JJ, Sterling T, Mysinger MM, Bolstad ES & Coleman RG (2012). ZINC: a free tool to discover chemistry for biology. *J Chem Inf Model* **52**, 1757–1768.

James AF, Choisy SCM & Hancox JC (2007). Recent advances in understanding sex differences in cardiac repolarization. *Prog Biophys Mol Biol* **94**, 265–319.

Janse de Jonge XA, Boot CR, Thom JM, Ruell PA & Thompson MW (2001). The influence of menstrual cycle phase on skeletal muscle contractile characteristics in humans. *J Physiol* **530**, 161–166.

Jo S, Kim T, Iyer VG & Im W (2008). CHARMM-GUI: a web-based graphical user interface for CHARMM. *J Comput Chem* **29**, 1859–1865.

Jorgensen WL, Chandrasekhar J, Madura JD, Impey RW & Klein ML (1983). Comparison of simple potential functions for simulating liquid water. *J Chem Phys* **79**, 926–935.

Jose AD & Collison D (1970). The normal range and determinants of the intrinsic heart rate in man. *Cardiovasc Res* **4**, 160–167.

Kim JA, Lopes CM, Moss AJ, McNitt S, Barsheshet A, Robinson JL, Zareba W, Ackerman MJ, Kaufman ES, Towbin JA, Vincent M & Goldenberg I (2010). Trigger-specific risk factors and response to therapy in long QT syndrome type 2. *Heart Rhythm* **7**, 1797–1805.

Klauda JB, Venable RM, Freites JA, O'Connor JW, Tobias DJ, Mondragon-Ramirez C, Vorobyov I, MacKerell AD Jr & Pastor RW (2010). Update of the CHARMM all-atom additive force field for lipids: validation on six lipid types. *J Phys Chem B* **114**, 7830–7843.

Kopp J & Schwede T (2004). The SWISS-MODEL Repository of annotated three-dimensional protein structure homology models. *Nucleic Acids Res* **32**, D230–D234.

Kurokawa J, Sasano T, Kodama M, Li M, Ebana Y, Harada N, Honda S, Nakaya H & Furukawa T (2015). Aromatase knockout mice reveal an impact of estrogen on drug-induced alternation of murine electrocardiography parameters. *J Toxicol Sci* **40**, 339–348.

Kurokawa J, Suzuki T & Furukawa T (2009). New aspects for the treatment of cardiac diseases based on the diversity of functional controls on cardiac muscles: acute effects of female hormones on cardiac ion channels and cardiac repolarization. *J Pharmacol Sci* **109**, 334–340.

Kurokawa J, Tamagawa M, Harada N, Honda S, Bai CX, Nakaya H & Furukawa T (2008). Acute effects of oestrogen on the guinea pig and human IKr channels and drug-induced prolongation of cardiac repolarization. *J Physiol* **586**, 2961–2973.

Lanfranchi PA, Ackerman MJ, Kara T, Shamsuzzaman AS, Wolk R, Jurak P, Amin R & Somers VK (2010). Gene-specific paradoxical QT responses during rapid eye movement sleep in women with congenital long QT syndrome. *Heart Rhythm* **7**, 1067–1074.

Lees-Miller JP, Duan Y, Teng GQ & Duff HJ (2000). Molecular determinant of high-affinity dofetilide binding to *HERG1* expressed in *Xenopus* oocytes: involvement of S6 sites. *Mol Pharmacol* **57**, 367–374.

Lees-Miller JP, Guo J, Wang Y, Perissinotti LL, Noskov SY & Duff HJ (2015). Ivabradine prolongs phase 3 of cardiac repolarization and blocks the hERG1 (KCNH2) current over a concentration-range overlapping with that required to block HCN4. *J Mol Cell Cardiol* **85**, 71–78.

Lehmann MH, Hardy S, Archibald D, Quart B & MacNeil DJ (1996). Sex difference in risk of torsade de pointes with d,l-sotalol. *Circulation* **94**, 2535–2541.

Liu CC, Kuo TB & Yang CC (2003). Effects of estrogen on gender-related autonomic differences in humans. *Am J Physiol Heart Circ Physiol* **285**, H2188–H2193.

Liu T, Choi B-R, Drici M-D & Salama G (2005). Sex modulates the arrhythmogenic substrate in prepubertal rabbit hearts with Long QT 2. *J Cardiovasc Electrophysiol* **16**, 516–524.

Locati EH, Zareba W, Moss AJ, Schwartz PJ, Vincent GM, Lehmann MH, Towbin JA, Priori SG, Napolitano C, Robinson JL, Andrews M, Timothy K & Hall WJ (1998). Age- and sex-related differences in clinical manifestations in patients with congenital long-QT syndrome: findings from the International LQTS Registry. *Circulation* **97**, 2237–2244.

Lou Q, Fedorov VV, Glukhov AV, Moazami N, Fast VG & Efimov IR (2011). Transmural heterogeneity and remodeling of ventricular excitation-contraction coupling in human heart failure. *Circulation* **123**, 1881–1890.

MacKerell AD, Bashford D, Bellott M, Dunbrack RL, Evanseck JD, Field MJ, Fischer S, Gao J, Guo H, Ha S, Joseph-McCarthy D, Kuchnir L, Kuczera K, Lau FTK, Mattos C, Michnick S, Ngo T, Nguyen DT, Prodhom B, Reiher WE, Roux B, Schlenkrich M, Smith JC, Stote R, Straub J, Watanabe M, Wiorkiewicz-Kuczera J, Yin D & Karplus M (1998). All-atom empirical potential for molecular modeling and dynamics studies of proteins. *J Phys Chem B* **102**, 3586–3616.

Magnano AR, Holleran S, Ramakrishnan R, Reiffel JA & Bloomfield DM (2002). Autonomic nervous system influences on QT interval in normal subjects. *J Am Coll Cardiol* **39**, 1820–1826.

Makkar RR, Fromm BS, Steinman RT, Meissner MD & Lehmann MH (1993). Female gender as a risk factor for torsades de pointes associated with cardiovascular drugs. *J Am Med Assoc* **270**, 2590–2597.

Mitcheson JS, Chen J & Sanguinetti MC (2000). Trapping of a methanesulfonanilide by closure of the HERG potassium channel activation gate. *J Gen Physiol* **115**, 229–240.

Moss AJ, Robinson JL, Gessman L, Gillespie R, Zareba W, Schwartz PJ, Vincent GM, Benhorin J, Heilbron EL, Towbin JA, Priori SG, Napolitano C, Zhang L, Medina A, Andrews ML & Timothy K (1999). Comparison of clinical and genetic variables of cardiac events associated with loud noise versus swimming among subjects with the long QT syndrome. *Am J Cardiol* **84**, 876–879.

Munro CJ, Stabenfeldt GH, Cragun JR, Addiego LA, Overstreet JW & Lasley BL (1991). Relationship of serum estradiol and progesterone concentrations to the excretion profiles of their major urinary metabolites as measured by enzyme immunoassay and radioimmunoassay. *Clin Chem* **37**, 838–844.

Nakagawa M, Ooie T, Ou B, Ichinose M, Takahashi N, Hara M, Yonemochi H & Saikawa T (2005). Gender differences in autonomic modulation of ventricular repolarization in humans. *J Cardiovasc Electrophysiol* **16**, 278–284.

Nakagawa M, Ooie T, Takahashi N, Taniguchi Y, Anan F, Yonemochi H & Saikawa T (2006). Influence of menstrual cycle on QT interval dynamics. *Pacing Clin Electrophysiol* **29**, 607–613.

Nakajo K, Ulbrich MH, Kubo Y & Isacoff EY (2010). Stoichiometry of the KCNQ1 – KCNE1 ion channel complex. *Proc Natl Acad Sci USA* **107**, 18862–18867.

Nakamura H, Kurokawa J, Bai C-X, Asada K, Xu J, Oren RV, Zhu ZI, Clancy CE, Isobe M & Furukawa T (2007). Progesterone regulates cardiac repolarization through a nongenomic pathway: an in vitro patch-clamp and computational modeling study. *Circulation* **116**, 2913–2922.

Noskov SY, Berneche S & Roux B (2004). Control of ion selectivity in potassium channels by electrostatic and dynamic properties of carbonyl ligands. *Nature* **431**, 830–834.

Noskov SY & Roux B (2008). Control of ion selectivity in LeuT: Two Na$^+$ binding sites with two different mechanisms. *J Mol Biol* **377**, 804–818.

O'Hara T & Rudy Y (2012). Arrhythmia formation in subclinical ("silent") long QT syndrome requires multiple insults: quantitative mechanistic study using the KCNQ1 mutation Q357R as example. *Heart Rhythm* **9**, 275–282.

O'Hara T, Virag L, Varro A & Rudy Y (2011). Simulation of the undiseased human cardiac ventricular action potential: model formulation and experimental validation. *PLoS Comput Biol* **7**, e1002061.

Pages G, Torres AM, Ju P, Bansal PS, Alewood PF, Kuchel PW & Vandenberg JI (2009). Structure of the pore-helix of the hERG K$^+$ channel. *Eur Biophys J* **39**, 111–120.

Perrin MJ, Kuchel PW, Campbell TJ & Vandenberg JI (2008). Drug binding to the inactivated state is necessary but not sufficient for high-affinity binding to human *ether-à-go-go*-related gene channels. *Mol Pharmacol* **74**, 1443–1452.

Perry M, de Greoot MJ, Helliwell R, Leishman D, Tristani-Firouzi M, Sanguinetti MC & Mitcheson J (2004). Structural determinants of HERG channel block by clofilium and ibutilide. *Mol Pharmacol* **66**, 240–249.

Pham TV, Robinson RB, Danilo JP & Rosen MR (2002). Effects of gonadal steroids on gender-related differences in transmural dispersion of L-type calcium current. *Cardiovasc Res* **53**, 752.

Pham TV & Rosen MR (2002). Sex, hormones, and repolarization. *Cardiovasc Res* **53**, 740–751.

Pham TV, Sosunov EA, Gainullin RZ, Danilo P Jr & Rosen MR (2001). Impact of sex and gonadal steroids on prolongation of ventricular repolarization and arrhythmias induced by I_K-blocking drugs. *Circulation* **103**, 2207–2212.

Phillips JC, Braun R, Wang W, Gumbart J, Tajkhorshid E, Villa E, Chipot C, Skeel RD, Kale L & Schulten K (2005). Scalable molecular dynamics with NAMD. *J Comput Chem* **26**, 1781–1802.

Robertson JL, Palmer LG & Roux B (2008). Long-pore electrostatics in inward-rectifier potassium channels. *J Gen Physiol* **132**, 613–632.

Rodriguez I, Kilborn MJ, Liu XK, Pezzullo JC & Woosley RL (2001). Drug-induced QT prolongation in women during the menstrual cycle. *J Am Med Assoc* **285**, 1322–1326.

Rodriguez-Menchaca A, Ferrer-Villada T, Lara J, Fernandez D, Navarro-Polanco RA & Sanchez-Chapula JA (2006). Block of HERG channels by berberine: mechanisms of voltage- and state-dependence probed with site-directed mutant channels. *J Cardiovasc Pharmacol* **47**, 21–29.

Romero L, Trenor B, Yang PC, Saiz J & Clancy CE (2014). In silico screening of the impact of hERG channel kinetic abnormalities on channel block and susceptibility to acquired long QT syndrome. *J Mol Cell Cardiol* **72**, 126–137.

Salama G & Bett GC (2014). Sex differences in the mechanisms underlying long QT syndrome. *Am J Physiol Heart Circ Physiol* **307**, H640–H648.

Shimoni Y, Emmett T, Schmidt R, Nygren A & Kargacin G (2009). Sex-dependent impairment of cardiac action potential conduction in type 1 diabetic rats. *Am J Physiol Heart Circ Physiol* **296**, H1442–H1450.

Sims C, Reisenweber S, Viswanathan PC, Choi B-R, Walker WH & Salama G (2008). Sex, age, and regional differences in L-type calcium current are important determinants of arrhythmia phenotype in rabbit hearts with drug-induced long QT type 2. *Circ Res* **102**, e86–e100.

Smetana P, Batchvarov VN, Hnatkova K, Camm AJ & Malik M (2002). Sex differences in repolarization homogeneity and its circadian pattern. *Am J Physiol Heart Circ Physiol* **282**, H1889–H1897.

Stansfeld PJ, Gedeck P, Gosling M, Cox B, Mitcheson JS & Sutcliffe MJ (2007). Drug block of the hERG potassium channel: Insight from modeling. *Proteins* **68**, 568–580.

Stary A, Wacker SJ, Boukharta L, Zachariae U, Karimi-Nejad Y, Aqvist J, Vriend G & de Groot BL (2010). Toward a consensus model of the HERG potassium channel. *ChemMedChem* **5**, 455–467.

Stork D, Timin EN, Berjukow S, Huber C, Hohaus A, Auer M & Hering S (2007). State dependent dissociation of HERG channel inhibitors. *Br J Pharmacol* **151**, 1368–1376.

Stramba-Badiale M, Locati EH, Martinelli A, Courville J & Schwartz PJ (1997). Gender and the relationship between ventricular repolarization and cardiac cycle length during 24-h Holter recordings. *Eur Heart J* **18**, 1000–1006.

Tadros R, Ton AT, Fiset C & Nattel S (2014). Sex differences in cardiac electrophysiology and clinical arrhythmias: epidemiology, therapeutics, and mechanisms. *Can J Cardiol* **30**, 783–792.

Thompson JD, Higgins DG & Gibson TJ (1994). CLUSTAL-W: improving the sensitivity of progressive multiple sequence alignment through sequence weighting, position-specific gap penalties and weight matrix choice. *Nucleic Acids Res* **22**, 4673–4680.

Vandenberg JI, Walker BD & Campbell TJ (2001). HERG K^+ channels: friend and foe. *Trends Pharmacol Sci* **22**, 240–246.

Van Opstal JM, Leunissen JD, Wellens HJ & Vos MA (2001). Azimilide and dofetilide produce similar electrophysiological and proarrhythmic effects in a canine model of Torsade de Pointes arrhythmias. *Eur J Pharmacol* **412**, 67–76.

Vaseghi M & Shivkumar K (2008). The role of the autonomic nervous system in sudden cardiac death. *Prog Cardiovasc Dis* **50**, 404–419.

Wang YB, Guo JQ, Perissinotti LL, Lees-Miller J, Teng GQ, Durdagi S, Duff HJ & Noskov SY (2016). Role of the pH in state-dependent blockade of hERG currents. *Sci Rep* **6**, 32536.

Whicher JR & MacKinnon R (2016). Structure of the voltage-gated K^+ channel Eag1 reveals an alternative voltage sensing mechanism. *Science* **353**, 664–669.

Wilde AA, Jongbloed RJ, Doevendans PA, Duren DR, Hauer RN, van Langen IM, van Tintelen JP, Smeets HJ, Meyer H & Geelen JL (1999). Auditory stimuli as a trigger for arrhythmic events differentiate HERG-related (LQTS2) patients from KVLQT1-related patients (LQTS1). *J Am Coll Cardiol* **33**, 327–332.

Xie Y, Sato D, Garfinkel A, Qu Z & Weiss JN (2010). So little source, so much sink: requirements for afterdepolarizations to propagate in tissue. *Biophys J* **99**, 1408–1415.

Yang PC & Clancy CE (2012). In silico prediction of sex-based differences in human susceptibility to cardiac ventricular tachyarrhythmias. *Front Physiol* **3**, 360.

Yang PC, Kurokawa J, Furukawa T & Clancy CE (2010). Acute effects of sex steroid hormones on susceptibility to cardiac arrhythmias: a simulation study. *PLoS Comput Biol* **6**, e1000658.

Yang X, Chen G, Papp R, Defranco DB, Zeng F & Salama G (2012). Oestrogen upregulates L-type Ca^{2+} channels via oestrogen-receptor-α by a regional genomic mechanism in female rabbit hearts. *J Physiol* **590**, 493–508.

Yesselman JD, Price DJ, Knight JL & Brooks CL (2012). MATCH: an atom-typing toolset for molecular mechanics force fields. *J Comput Chem* **33**, 189–202.

Young RJ & Panfilov AV (2010). Anisotropy of wave propagation in the heart can be modeled by a Riemannian electrophysiological metric. *Proc Natl Acad Sci USA* **107**, 15063–15068.

Zachariae U, Giordanetto F & Leach AG (2009). Side chain flexibilities in the human ether-a-go-go related gene potassium channel (hERG) together with matched-pair binding studies suggest a new binding mode for channel blockers. *J Med Chem* **52**, 4266–4276.

Additional information

Competing interests

None.

Author contributions

P.-C.Y., L.L.P., and S.N. designed and performed simulations, analysed data, and prepared the manuscript; Y.W. and M.-T.J. designed and performed simulations; F.L-R. and J.K. designed and performed experiments; K.R.D. and I.V. analysed data, and revised the manuscript; R.D.H drafted the manuscript; C.E.C. designed simulations and experiments, analysed data, coordinated and oversaw the project, and prepared the manuscript. All authors approved the final submitted version.

Funding